Soils and Rocks

An International Journal of Geotechnical and Geoenvironmental Engineering

www.soilsandrocks.com

ISSN 1980-9743
ISSN-e 2675-5475

Gravitational mass movements in Brazil: causes, consequences, and solutions

Roberto Quental Coutinho[1#], Mauricio Ehrlich[2], Marcos Massao Futai[3], Luiz Antônio Bressani[4], Willy Alvarenga Lacerda[2], Bruno Diego de Morais[1]

Review Article

Keywords
Gravitational mass movements
Extreme rainfall
Climate change
Slope stability
Geotechnical engineering

Abstract

Gravitational mass movements are recurring phenomena in Brazil, causing significant environmental impacts as well as human, social, and economic losses. Data on gravitational mass movement occurrences between 1988 and 2022 recorded 959 events in 16 Brazilian states, resulting in a total of 4,146 victims. Extreme rainfall events in recent years, particularly in Santa Catarina, Rio de Janeiro, Bahia, Minas Gerais, Pernambuco, São Paulo, and Rio Grande do Sul, suggest an increase in consequences due to climate change. Considering this scenario, this article analyzes case studies in states such as Pernambuco, Rio de Janeiro, São Paulo, Paraná, and Rio Grande do Sul, addressing causes, impacts, rupture mechanisms, and adopted solutions. Geological-geotechnical investigations, numerical analyses, and continuous monitoring have been crucial in understanding rupture mechanisms and proposing mitigating solutions. The studies identified geological and geomorphological conditions as the main predisposing factors, while inadequate human actions, insufficient investigation in infrastructure projects, and rainwater infiltration were found to be the primary aggravating and triggering factors. Therefore, with the increased frequency of extreme rainfall, it is essential to adopt new approaches that consider the impacts of these events in urban occupation and infrastructure projects, reinforcing preventive and adaptive strategies to reduce future risks.

1. Introduction

Gravitational Mass Movements (GMM) are complex and among the costliest natural hazards, causing environmental damage, economic losses, and social impacts, including fatalities, injuries, and displacement (Lu & Godt, 2013). Between 1970 and 2019, GMM accounted for 6% of recorded disasters and 1% of global economic losses (WMO, 2021). From 2004 to 2016, these events on a global scale caused 55,997 deaths in 4,862 incidents, averaging over 4,000 deaths per year (Froude & Petley, 2018).

In Brazil, GMM are frequent and result from natural and human-induced factors. Rainfall is the primary trigger, increasing soil stress and reducing resistance (Augusto Filho et al., 2018). Macedo & Sandre (2022) identify mass movements as the leading cause of geological disaster fatalities in Brazil. Between 1988 and 2022, 959 events were recorded in 16 states, with 4,146 victims. The states with the highest number of fatalities were Rio de Janeiro, São Paulo, and Minas Gerais, among others. Given the increasing frequency and severity of these events, updated data is necessary.

The past decades have seen a rise in GMM-related disasters in Brazil. Intense rainfall during the months of September, October and November; in November 2008, a great disaster occurred in Gaspar, Santa Catarina, causing several GMM and generalized inundation. One GMM caused the disruption and local fire in Bolivia–Brazil Gas Pipeline (GASBOL). From 21 to 24 of November the total rainfall was 514,9 mm. A total of 28,000 displaced individuals and 40 deaths were the result (Bauzys, 2010).

The past decades have seen a rise in GMM-related disasters in Brazil. One of the most devastating disasters

[#]Corresponding author. E-mail address: roberto.coutinho@ufpe.br
[1]Universidade Federal de Pernambuco, Departamento de Engenharia Civil, Recife, PE, Brazil.
[2]Universidade Federal do Rio de Janeiro, Departamento de Engenharia Civil, Rio de Janeiro, RJ, Brazil.
[3]Universidade de São Paulo, Escola Politécnica, São Paulo, SP, Brazil.
[4]Universidade Federal do Rio Grande do Sul, Departamento de Engenharia Civil, Porto Alegre, RS, Brazil.

Submitted on January 31, 2025; Final Acceptance on May 21, 2025; Discussion open until November 30, 2025.

Editor: Renato P. Cunha

https://doi.org/10.28927/SR.2025.001625

This is an Open Access article distributed under the terms of the Creative Commons Attribution license (https://creativecommons.org/licenses/by/4.0/), which permits unrestricted use, distribution, and reproduction in any medium, provided the original work is properly cited.

occurred in the Mountain Region of Rio de Janeiro in January 2011, where intense rains triggered landslides and floods. The disaster resulted in 918 deaths, 22,604 displaced individuals, and 8,795 homeless people (Alves et al., 2022). Seven municipalities declared a state of calamity, with Teresópolis, Nova Friburgo, and Petrópolis experiencing the most severe impacts (Banco Mundial, 2012). In response, the federal government established CEMADEN, the National Center for Natural Disaster Monitoring and Alerts, to improve early warnings (Rosi et al., 2019).

In 2022, MR-Recife in Pernambuco recorded over 200 mm of rainfall in 24 hours, triggering landslides that caused 133 fatalities (Marengo et al., 2023; Recife, 2023). That same year, Santa Catarina saw similar rainfall levels, while in February 2023, the São Paulo coast experienced a record 600 mm of rain in 24 hours, leading to 65 deaths and displacing around 2,000 people (Costa, 2023).

Between May and June of 2024, Rio Grande do Sul faced a severe climate catastrophe. In the Lake Guaíba basin, rainfall between April 27 and May 19 ranged from 300 to 900 mm, causing extensive flooding and mass movements that affected 2.4 million people (Rio Grande do Sul, 2024).

Gariano & Guzzetti (2016) emphasize that while climate change is known to impact slope stability, uncertainties remain regarding landslide frequency and intensity in response to climate projections. These gaps highlight the need for improved monitoring, early warning systems, and mitigation strategies.

This study examines case studies on mass movements in Brazil, analyzing their causes, impacts, and responses. It evaluates mitigation and stabilization strategies, emphasizing the importance of geological-geotechnical investigations, modeling, and continuous monitoring. Future publications will provide further insights into the 2022 MR-Recife and 2024 Rio Grande do Sul events.

2. Types and causes of gravitational mass movements

Gravitational mass movements (GMM) involve the downward displacement of rocks, soil, and debris due to gravity, often triggered by water infiltration, earthquakes, or increased pore pressure (Bromhead, 1992; Highland & Bobrowsky, 2008). The primary driving force is the material's potential energy, influenced by elevation and slope, with water acting as a key triggering factor (Goudie, 2004). Unlike erosion, GMM creates a rupture surface separating the displaced mass from the intact material (Lu & Godt, 2013).

Given their complexity, GMM studies require an integrated approach combining engineering, geology, and geomorphology. Classification systems have evolved to standardize terminology, with Varnes' (1978) system widely accepted and later refined by Cruden & Varnes (1996). In Brazil, adaptations to tropical environments were made by Augusto Filho (1992). Hungr et al. (2014) further expanded the classification, replacing the traditional threefold material division with a more detailed categorization (e.g., clay, mud, sand, ice), defining six movement types (falls, overturns, slides, lateral expansions, flows, and slope deformations) and formalizing 32 movement types.

In Brazil, GMM is influenced by precipitation patterns, substrate composition, slope characteristics, and human activities like excavation and deforestation (Augusto Filho et al., 2018). The geotechnical characterization of GMM considers three main causative factor groups (Leroueil et al., 1996): predisposing (geology, morphology, anthropogenic), triggering (rainfall, earthquakes, erosion), and aggravating (altering stability or speed). Cruden & Varnes (1996) classify causes into geological (weak sediments, structural discontinuities), morphological (erosion, vegetation loss), physical (heavy rainfall, seismic activity), and anthropogenic (excavations, deforestation).

3. Presentation of case studies

In this item, case studies related to geotechnical investigation, monitoring, stability analysis, and slope and hillside stabilization solutions in different states of Brazil will be presented, with a specific focus on municipalities in the states of Pernambuco, Rio de Janeiro, São Paulo, Paraná, and Rio Grande do Sul.

3.1 Case studies of the state of Pernambuco

This subitem presents studies carried out in the state of Pernambuco, focusing on a section of PE-89 highway, in the municipality of Machados; geological-geotechnical investigations, instrumentation and modeling of occupied slopes in Camaragibe; and a summary of the disaster caused by the rains at the end of May 2022 in the Metropolitan Region of Recife.

3.1.1 Analysis of the landslide failure mechanism on the slope of the PE-89 Highway in the municipality of Machado

This study aimed to carry out a geological-geotechnical investigation of the materials (soil/rock) and evaluate the stability of the slope and understand the rupture mechanism of a landslide that occurred on a slope located on the PE-89 highway, in the municipality of Machados, state of Pernambuco, Brazil. For more details about this study, see Coutinho et al. (2000).

The natural slope investigated is composed of residual gneiss soil and weathered rock, with an average slope of 35°. The landslide involved a ruptured surface 170 meters long and 80 meters wide, in a region with a hot and humid climate, with a rainy season between April and August. The field investigation, shown in Figure 1, included topographic survey, geological mapping, percussion survey test Standard Penetration Tests (SPT) and Rock Quality Designation test (RQD), vertical trenches, moisture content analyses and collection of soil and rock samples from areas A1 to A6.

CC BY

3.1.1.1 Geological-geotechnical investigation

Exploration of the subsoil revealed that the mature residual soil presents porous sandy clay 2 meters thick, while the young residual soil is formed by silty-clay sand with mica, up to 15 meters thick, preserving characteristics of the matrix rock (Figure 2a). The results of the geotechnical investigation suggest that the failure surface corresponds to the soil-rock contact.

Humidity and hydraulic conductivity studies showed variations in moisture content between 10% and 24%, with greatest changes at 2 m depth in the mature soil and at 4 m at the top of the landslide. Moisture content profiles were periodically monitored in Areas 1, 2 and 3a, with samples collected by manual auger, to analyze the variation between the dry and rainy seasons (Figure 2b). The results indicated values between 10% and 24%, with a progressive reduction in depth. On the slope, the greatest variations occurred around 2 m (mature residual soil), while at the top of the landslide area, they occurred up to around 4 m.

Saturated hydraulic conductivity was higher in mature soil (K_{sat} =1.1 ± 0.48 x 10^{-5} m/s) than in young soil (K_{sat} = 0.41 ± 0.15 x 10^{-5} m/s), reflecting its granular and porous structure (Figure 2c). These results highlight the complexity of the hydraulic and structural behavior of the soils involved in the landslide.

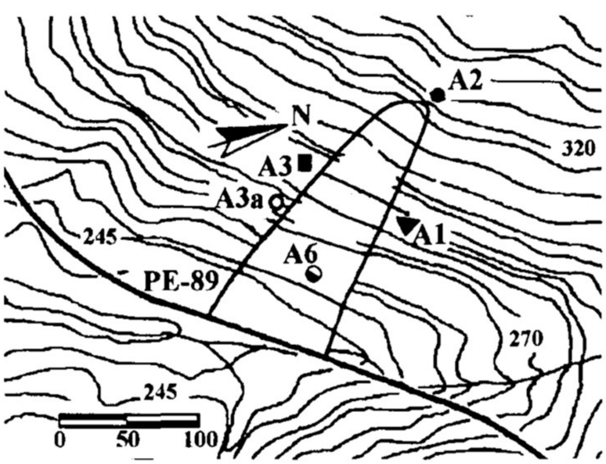

Figure 1. Investigated areas (A1 to A6).

The laboratory investigation revealed that the mature residual soil had 40% clay and a Plasticity Index (PI) of 12 to 20%, while the young soil showed 70% sand, a plasticity index of 6 to 16% and a high presence of mica (40 to 50%). Studies indicate that mineralogy, especially the proportions of mica and feldspar, significantly affect shear strength.

The soil-water retention curve was obtained by pressure plate testing on undisturbed samples in the laboratory. During the rainy period of 1995, field suction values, measured by the filter paper method on young residual soils, ranged from 10 to 80 kPa. In the laboratory, the initial suction in the tests was estimated between 20 and 70 kPa, in line with values observed in the field.

Direct shear tests were performed on samples that were both flooded and with natural moisture content, and the results are presented in Table 1. The samples were prepared in directions parallel and perpendicular to the foliation to assess drained shear strength parameters and the influence of anisotropy. The young residual soils exhibited an effective friction angle (ϕ') ranging from 29.3° to 31.4° (average of 30°) and effective cohesion (c') ranging from 2.8 to 7.0 kPa in Area 1 and from 0 to 38.3 kPa in Area 3. The highest cohesion values were observed in samples with natural moisture content, while the lowest values occurred in flooded samples parallel to the foliation. The similarity between the parameters obtained in the two areas was noted, although Area 3 showed a greater influence of suction and anisotropy.

The flooded samples prepared perpendicular to the foliation exhibited higher c' values, confirming the influence of anisotropy, especially in the soils of Area 3. Predisposing factors, such as the orientation of the foliations parallel to the direction of the slope and the high mica content, may contribute to adverse discontinuities in the soil mass.

3.1.1.2 Methodological procedures for flow and stability analyses

The stability of the slope was analyzed in two stages: a flow analysis, considering the rainfall history before failure, and a limit equilibrium analysis applying the Sarma model using the distribution of pore pressures obtained in the flow

Table 1. Strength parameters - conventional direct shear.

Site	Soil	Depth (m)	Foliation	Test Condition	c' (kPa)	ϕ' (°)
Area 1	Mature Residual	0.75	--------	Submerged	10.8	31.9
			--------	Nat. M. C	71.4	41.6
	Young Residual	8.7	Parallel	Submerged	2.8	29.3
			Perpendicular	Submerged	5.3	31.4
			Parallel	Nat. M. C	7	29.5
Area 3	Mature Residual	1.9	--------	Submerged	0	35.5
				Nat. M. C	15.8	37.8
	Young Residual	5.6	Parallel	Submerged	0	30.5
		4.6	Perpendicular	Submerged	10.2	30.3

CC BY

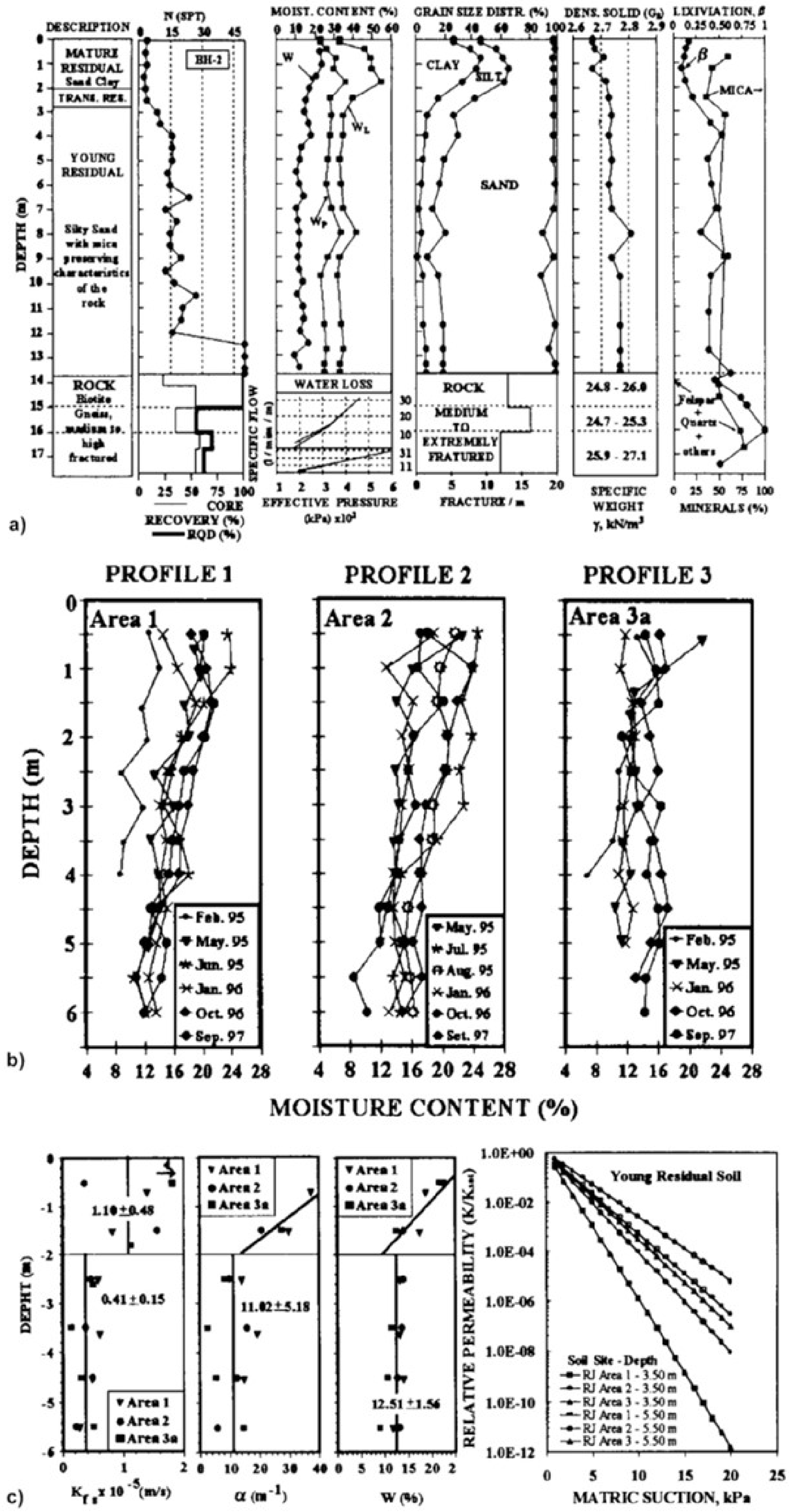

Figure 2. Results of the geotechnical investigation: (a) Result of a borehole (SPT/RQD) and characteristic properties - Area 1; (b) Moisture content profiles - Areas 1, 2 and 3a; (c) Results of permeability test (Guelph permeameter).

analysis. Two conditions were evaluated: the cross section before the construction of the road (natural condition) and after construction (rupture condition).

For the rupture condition, two scenarios were considered: sliding in a single stage (cross section 2 - Figure 3a) or in two stages, involving movements at the foot and at the top of the slope (cross sections 10-8 - Figure 3a). Figure 3b presents the typical soil profile/cross section for the case of a single-stage landslide (section 2).

3.1.1.3 Flow analyses

In the flow analyses, due to uncertainty about the initial suction during the rupture period, a parametric study was conducted with initial suction varying between 4 and 60 kPa, a range compatible with field measurements during the rainy season. The analysis used previously described geotechnical parameters and considered the hydraulic conductivity of the saprolite to be greater than or equal to that of the young residual soil.

Two behaviors were identified: i) for initial suction ≤10 kPa, infiltration saturated the top of the rock, generating positive pore pressure along the impermeable surface; ii) for initial suction >10 kPa, infiltration kept the slope in an unsaturated condition, with negative pore pressure. These results illustrate the impact of initial suction on the hydro-mechanical behavior of the slope.

3.1.1.4 Stability analyses

The shear strength parameters used in the stability analysis were based on the direct shear tests performed (Figure 4a). For the saprolite, $c' = 20$ kPa and $\phi' = 45°$ were adopted. The parameter ϕ^b, associated with matric suction, was considered equal to ϕ' due to the low suction values recorded during the rainy season. The critical slip surface was investigated assuming a non-circular geometry, encompassing the observed failure.

Analysis revealed a continuous reduction in safety factor (*SF*) as initial suction decreased, with a steeper drop for suctions ≤ 10 kPa, due to positive pore pressure caused by

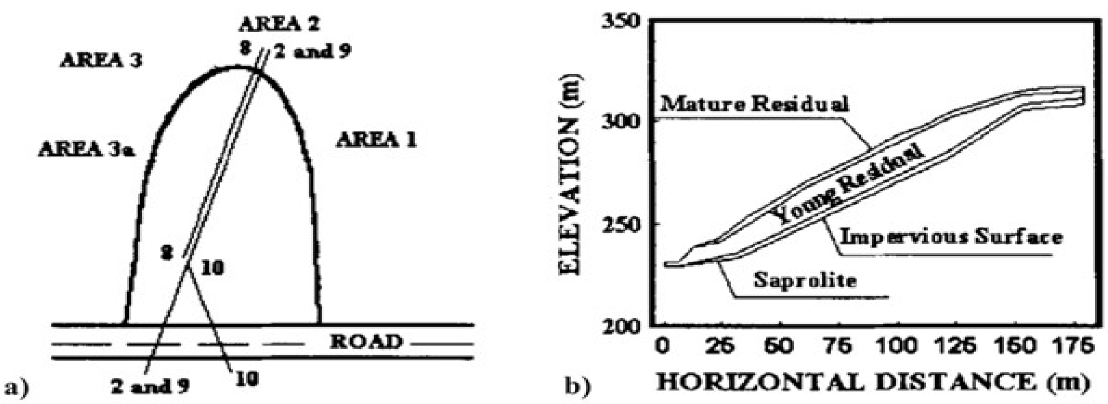

Figure 3. (a) Cross-sections-stability analysis; (b) Typical soil profile-cross section 2.

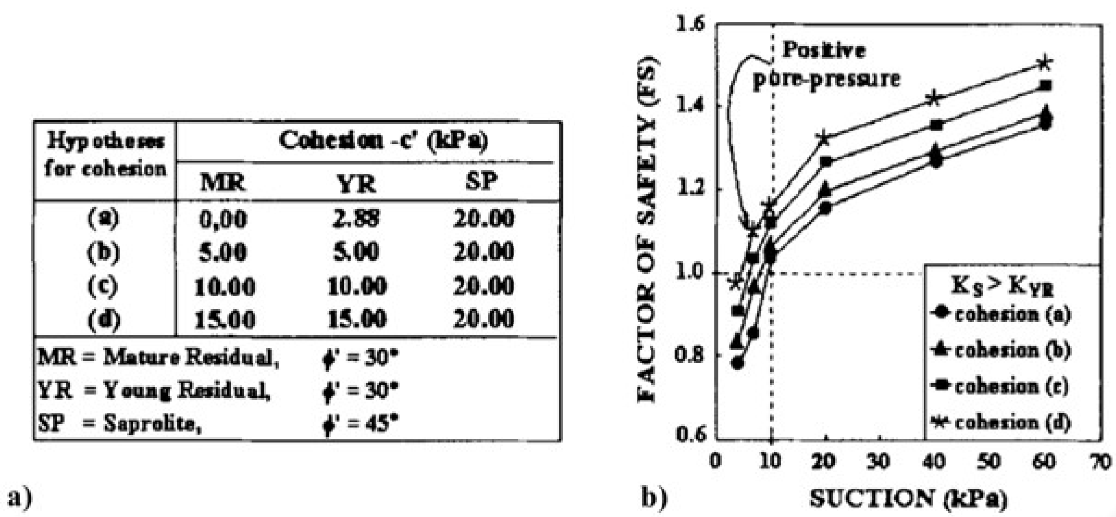

Hypotheses for cohesion	Cohesion -c' (kPa)		
	MR	YR	SP
(a)	0,00	2.88	20.00
(b)	5.00	5.00	20.00
(c)	10.00	10.00	20.00
(d)	15.00	15.00	20.00
MR = Mature Residual,	φ' = 30°		
YR = Young Residual,	φ' = 30°		
SP = Saprolite,	φ' = 45°		

Figure 4. (a) Strength parameters considered; (b) SF-Suction relationship (section 2).

CC BY

rain infiltration (Figure 4b). For hypotheses of $c' = 0$ - 5 kPa, the *SF* was close to 1.0 for suctions of 7 - 10 kPa, indicating imminent instability. Similar results were found for the sliding cases considering one and two stages. Cross section 9 showed that *SF* in the natural condition was 15% higher before road construction, highlighting the negative impact of the intervention on slope stability.

The calculated critical slip surfaces coincided with the faults observed in the field, reinforcing the modeling accuracy. The analysis suggests that the construction of the road contributed significantly to the reduction in *SF*, indicating that cuts and interventions on the slope were triggering factors for the landslide.

A retroanalysis was performed to evaluate the shear strength parameters, using the expression of apparent cohesion $c^* = c' + (u_a - u_w)\ tan\phi^b$, intending to correlate the results with the observed rupture. The results obtained for section 2, presented in Table 2, indicate that the resistance parameters determined in this analysis were consistent with those obtained in laboratory tests. The results confirm that the resistance parameters derived from laboratory tests are sufficient to explain the slope instability. This validates the reliability of the tests in reproducing the critical conditions that led to the failure.

3.1.1.5 Conceptual synthesis

The results of the geological-geotechnical investigation were coherent, as they showed discrete anisotropic behavior in submerged shear strength. Stability analysis revealed a low safety factor (1.15 – 1.20) during the rainy season, indicating significant risk of landslides due to low suction values. Predisposing factors include high mica content and slope-parallel foliation. Slope cutting was identified as the main aggravating factor, while heavy rainfall acted as the triggering factor.

3.1.2 Geological-geotechnical investigation, instrumentation, and stability analysis with emphasis on anthropogenic influence on the slopes of Camaragibe

This study describes the geological-geotechnical study of the occurrence of a mass movement on a slope in the municipality of Camaragibe, in the state of Pernambuco, Brazil. To characterize the landslide that occurred and understand its failure mechanism, a detailed investigation was conducted, which included the use of instrumentation, field surveys and laboratory tests, as illustrated in Figure 5. The study area presents disordered occupation at the top of the slope, widely impacted by human actions that compromise its stability, such as constructions in inappropriate locations, improper cuts, poorly compacted landfills, drilling of artesian wells on the edges of the slope and inadequate disposal of wastewater. For more details about this study, see Coutinho et al. (2019).

3.1.2.1 Geological-geotechnical investigation

Residences located at the top of the slope discharge water directly onto the land without a drainage system, with wastewater following preferential paths indicated by the red arrows in Figure 6.

Studies carried out in 2005 showed that anthropogenic disposal represents 35% of annual precipitation. Although the average flow rate of precipitation (5.73 mm/day) is greater than that of wastewater (0.70 mm/day), the flow of wastewater is constant throughout the year, while that of precipitation occurs at specific periods, according to the details shown in the graph in Figure 7.

The landslide site is in an area of residual soil that is a product of the weathering of the granite rock mass (referred to as GRS) and sediments of the Barreiras Formation (referred to as BFS) that form layers of predominantly clayey or sandy soils, susceptible to gravitational mass movements

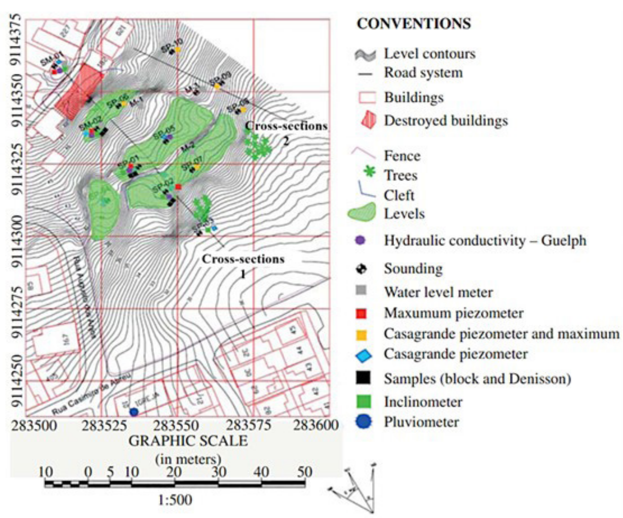

Figure 5. Topographic map of the area of study with the location of the field investigations in plan.

Table 2. Summary of the results of back-analysis to section 2.

Friction angle ϕ' (°)							
28.5		29.0		29.5		30.0	
c' (kPa)	*SF*	*c'* (kPa)	*SF*	*c'* (kPa)	*SF*	*c'* (kPa)	*SF*
5	1.019	3	1.007	3	1.003	1	1.024
7	1.046	5	1.039	5	1.024	3	1.044
					1.053	5	1.073

CC BY

and erosion processes in slope areas (Coutinho et al., 2006; Bandeira & Coutinho, 2015).

The boreholes conducted along the slope profile, with depths ranging from 12 to 20 meters, revealed varying soil types depending on the stratigraphic position. At the crest, layers of clayey sand over residual granite soil (GRS) predominate, characterized by high penetration resistance. In the intermediate region, the profiles are more heterogeneous, including silty sand, sandy clay, and consolidated residual soil layers. At the base, sandy soils with lower strength are predominant.

At the crest of the slope, boreholes SM-01 and SM-02 reached depths of 20 meters. The first borehole encountered the Barreiras Formation between 7 and 8 meters, with Standard Penetration Test (SPT) values ranging from 2 to 10 blows, indicating a relatively loose structure. Below this level, a sharp transition to young residual granite soil is marked by a significant increase in resistance, with SPT values rising to 65 blows/20 cm and 15 blows/1 cm, suggesting the presence of a more competent, heavily weathered material.

In the second borehole (SM-02), the Barreiras Formation was identified up to a depth of 7 meters, where a complete loss of water circulation was observed, indicating the presence of a highly fractured zone, marking the transition to residual

Figure 6. Wastewater direction (Coutinho et al., 2019).

granite soil. From this point onward, the SPT values increased significantly, reaching 33 blows/18 cm, requiring the use of rotary drilling methods.

The physical characterization of the soils showed that clay fractions tend to aggregate with other soil particles in their natural state, as evidenced by granulometric tests with and without deflocculant. The chemical tests indicated low levels of exchangeable bases, a typical characteristic of weathered kaolinitic soils. The mineralogical analysis revealed the presence of kaolinite, mica, and quartz, with quartz particles often coated with iron oxides, indicating the presence of lateritic soils. The soil-water retention curves showed typical sandy soil behavior for the *SF*B and a bimodal shape for the GRS, due to the presence of macropores and micropores.

The permeability tests classified the BFS and GRS as low and very low permeability soils, respectively. Direct shear tests revealed the plastic behavior of the soil under flooded conditions with a reduction in cohesion after the peak. Shear tests with suction control showed an increase in cohesion with suction.

The slope instrumentation included 25 Casagrande piezometers to monitor groundwater flow and five inclinometers to measure horizontal displacements. The piezometric levels remained high even during the dry season and varied with rainfall. The maximum displacement recorded by the inclinometer was 130 mm at SP-02, indicating failure near the contact between geological formations. The data also showed that accumulated rainfall in April 2005 triggered the first reactivation of the movement, followed by a second reactivation between May and August 2006 (Figure 8).

3.1.2.2 Methodological procedures for flow and stability analyses

To better understand the rupture mechanisms, the analysis of this case was divided into three stages: pre-failure, failure and reactivation. In the pre-failure stage, signs of instability were observed, such as cracks in homes since the year 2000. After the first rupture, geotechnical studies and instrumentation made

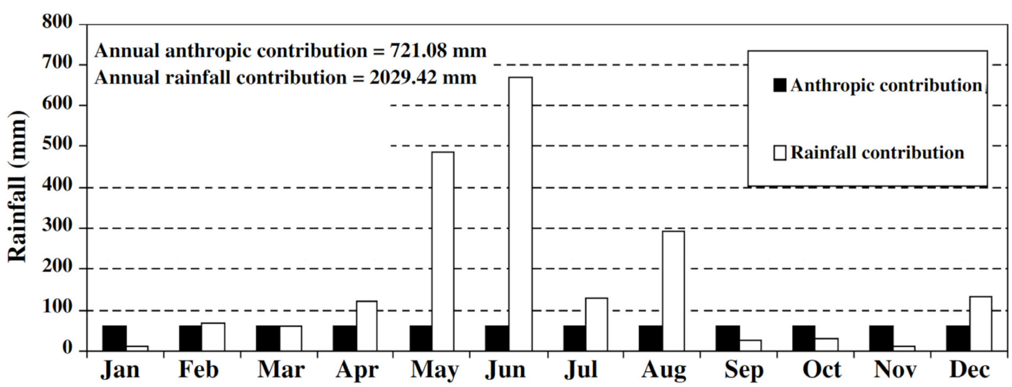

Figure 7. Annual anthropic contribution compared to the rainfall contribution in 2005.

CC BY

it possible to identify the geology, anthropogenic interventions (water cuts and disposal) and the relief as factors predisposing factors, while rain was the triggering factor.

The first rupture deposited material between points SP-01 and SP-02, generating overload and contributing to a second rupture. This process is illustrated in Figure 9a and 9b. The reactivation stage, which began in 2005, was triggered by intense rainfall of 100 mm, as indicated by the instrumentation. Horizontal displacements ranged from 80 to 100 mm, occurring in rigid blocks. The material involved was the same as the first rupture, demonstrating the unstable behavior of the colluvium resulting from the previous movements.

3.1.2.3 Flow analysis

The flow analysis, carried out with the SEEP/W and Slide 7.0 software, evaluated the slope pore pressures, considering the different permeability of the soils (Table 3). The permeability

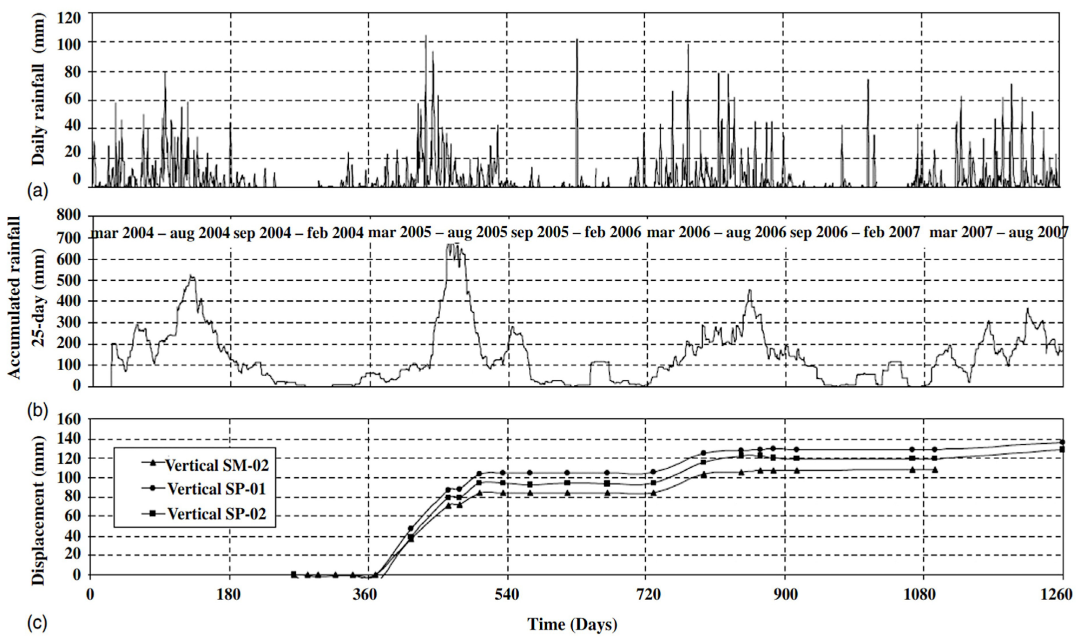

Figure 8. Horizontal mass movement displacements with accumulated rainfall over 25 days (Coutinho et al., 2019).

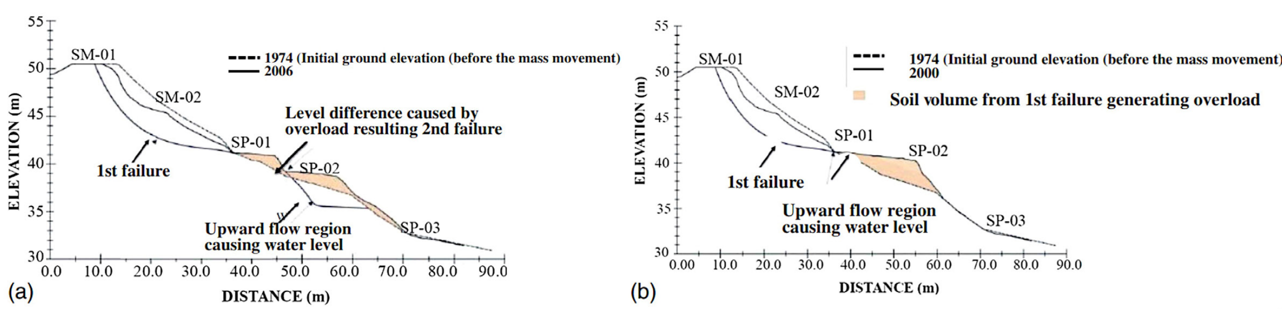

Figure 9. Failure mechanism occurring on hillside, referring to the failure stage.

Table 3. Soil, formation, and in situ permeability range used in the analyses.

Soil and formation	Range of K_{sat} (m/s)	K_{sat} adopted in analysis (m/s)
Soil w1: Variegated clayey sand—BFS	1.2 - 7.3 x 10^{-6}	3.88 x 10^{-6}
Soil 2: Yellow clayey sand—GRS	2.2 - 2.7 x 10^{-7}	2.52 x 10^{-7}
Soil 3: Grey sandy clay—GRS	1.10 x 10^{-7}	1.10 x 10^{-7}

Note: BFS = Barreiras Formation soil; and GRS = granite residual soil.

of residual mature granite soil (GRS) is one-tenth that of BFS soils, significantly reducing flow at the contact between geological formations. The analyses showed that between points SP-01 and SP-02, a high hydraulic load was detected, agreeing with the instrumentation results in this location, as an increase in positive pore pressure was observed due to rain.

3.1.2.4 Stability analyses

The analyses were carried out in three different scenarios: design phase, retroanalysis and reactivation using the SLOPE/W and Slide 7.0 software. The study used the limit equilibrium method and applied the Spencer, Morgenstern and Price, and Janbu models. In the design phase, the situation before the first rupture was simulated, with the original topography and an unknown rupture surface. In the retroanalysis, the rupture surface was defined based on the results of the instrumentation and flow analysis. In the reactivation phase, groundwater levels and post-rupture geometry were considered. The parameters used are presented in Table 4.

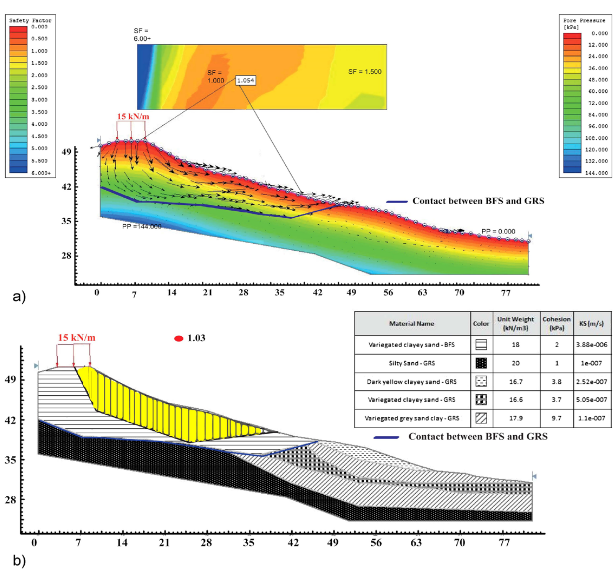

Figure 10. (a) Results of flow analysis and stability analysis–project phase–free calculation of the software covering the entire slope; (b) Stability analysis (failure stage) first failure between SM-02 and SP-01.

The stability analysis in the design phase sought to understand the instability process in the area, adopting the water level on the surface of the land as the most critical scenario. The analysis obtained a minimum safety factor of 1.05, indicating that the initial failure mechanism occurred at the top of the slope, between points SM-01 and SP-01, with the rupture surface located in the soil layer of the Barreiras Formation, confirming the limit between the two strata identified by inclinometers (Figure 10a).

The retroanalysis sought to understand the failure mechanism and evaluate the parameters that governed the movement, using original topography data, rupture surface defined by inclinometers and resistance parameters obtained in flooded conditions. It was concluded that the movement occurred in stages: the first break, with *SF* close to 1.00, occurred between points SM-02 and SP-01 (Figure 10b). The remaining material from the first rupture caused an overload on the slope, causing a second failure between SP-01 and SP-02, resulting in a *SF* of 1.047, justifying the observed movements.

In the analysis of the reactivation stage, the rupture surface, defined by inclinometers, occurred in blocks along the contact between the two geological formations. With the maximum water level, the safety factor (*SF*) of 1.060 justified the large displacements observed during intense rains, confirming precipitation as the main triggering factor. Already with the minimum water level, the *SF* of 1.983 indicated an apparently stable condition, corroborating the inclinometer records.

3.1.2.5 Proposed stabilization solution

Considering that the rise in the groundwater level is one of the main factors contributing to slope instability, the implementation of deep drainage was proposed through a line of deep horizontal drains (DHD) across the entire affected area. These drains were designed to be 40 meters long, spaced 5 meters apart, and inclined at 5°, in accordance with technical recommendations to ensure greater hydraulic efficiency. The drains were integrated into a surface drainage system aimed at directing rainwater away from the slope and reducing internal pore pressures. The stabilization solution also included the regrading of the slope to reduce its inclination.

In the upper portion of the slope, at specific locations identified as highly susceptible, stabilization was proposed

Table 4. Strength parameters adopted in stability analysis.

Implementation	Soil, depth (m), and formation	*c'* (kPa)	ϕ' (º)
Design Phase and Back-Analysis	SM-02 (1.5-1.8) BFS - Variegated clayey sand	2.00	33.00
	SP-01 (1.5-1.8) BFS - Dark yellow clayey sand	3.80	29.40
	SP-02 (1.5-1.8) GRS - Variegated clayey sand	3.70	312.00
	SP-02 (2.5-2.8) GRS - Variegated grey sandy clay	9.70	26.30
Reactivation Phase	Variegated clayey sand (1.5-1.8) BFS	0.0	30.3
	Variegated red and grey clayey sand (4.9-5.5) BFS	3.8	31.5
	Grey sandy clay (2.5-2.8) GRS	0.0	26.5
	Grey sandy clay (6.5-6.6) GRS	3.0	27.6

CC BY

using soil nailing combined with a shotcrete mesh facing. For surface protection and erosion control, grass cover was applied where feasible, particularly across the slope extension, while shotcrete mesh was used in specific areas more vulnerable to erosion or with extended occupation.

3.1.2.5 Conceptual synthesis

The study analyzed two distinct geological formations: the granite residual soil (GRS) and the Barreiras Formation soil (BFS), revealing significant differences in hydraulic conductivity, with the permeability of the GRS being ten times lower than that of the BFS, which promoted flows along their interfaces and contributed to slope instability. The stages of slope movement addressed — pre-failure, failure and reactivation — and the influence of anthropogenic factors, such as cuts and wastewater disposal, were highlighted. The initial failure was classified as a multiple superimposed rotational slip, triggered by intense rains that raised piezometric levels and generated positive pore pressures, causing mass movement in three stages. In the reactivation stage, instrumentation confirmed displacements in blocks, forming a continuous rupture surface. Laboratory and field tests corroborated the compatibility of the resistance parameters with the literature, while flow and stability analyses explained the failure mechanisms. Based on all the information gathered, a stabilization solution was proposed — although not implemented — consisting of the installation of deep horizontal drains, geometric reconfiguration of the slope with inclination reduction, surface protection using grass cover and shotcrete mesh, and, when necessary, the use of soil nailing.

3.1.3 3D stability analysis in alto do Padre Cícero – Camaragibe (PE)

Alto do Padre Cícero is a hillside located in the city of Camaragibe, MR-Recife, Pernambuco. In 2010, intense rain caused mass movements in the area. In this case study, 3D stability analyses are carried out to assess the safety of the slope, applying the limit equilibrium method and using the Slide3 software. For more details about this study, see Coutinho et al. (2020).

Alto do Padre Cícero is a slope densely occupied with soils from the Barreiras Formation, classified as high risk for landslides and erosion. The slope studied has been showing signs of instability since 2002. In June 2010, heavy rains resulted in an accumulated monthly volume of around 500 mm. In this scenario, after a storm, a landslide block and significant cracks formed at the top of the slope.

Furthermore, disorderly and informal occupations have advanced along the slope levels over the years. As a result, an increase in various human actions that favor the occurrence of mass movements can be observed on the natural slope, such as the disposal of solid waste, the carrying out of cuts and embankments without technical criteria, the disposal of wastewater on the surface and the increased overload on the slope due to housing construction.

3.1.3.1 Geological-geotechnical investigation

In this study, 06 Standard Penetration Tests (SPT), granulometry analyses, Atterberg limits, soil-water retention curves and shear strength determined by direct shear tests in natural and submerged conditions were performed.

The geotechnical profiles, based on the SPT tests and soil characterization, are presented in Figure 11. The top of the slope presents a surface layer of silty-sandy clay with consistencies ranging from soft to rigid. Next, there is a layer of silty-clayey sand whose resistance to penetration increases with depth. The water level on the date of the tests was found only in holes SPT 03 and SPT 06, with depths ranging from 4.00 to 5.00 m from the surface.

3.1.3.2 Stability analysis

To determine the Safety Factor (*SF*) of the slope, 2D and 3D stability analyses were performed using the Limit Equilibrium Method (LEM), implemented in the Slide2 and

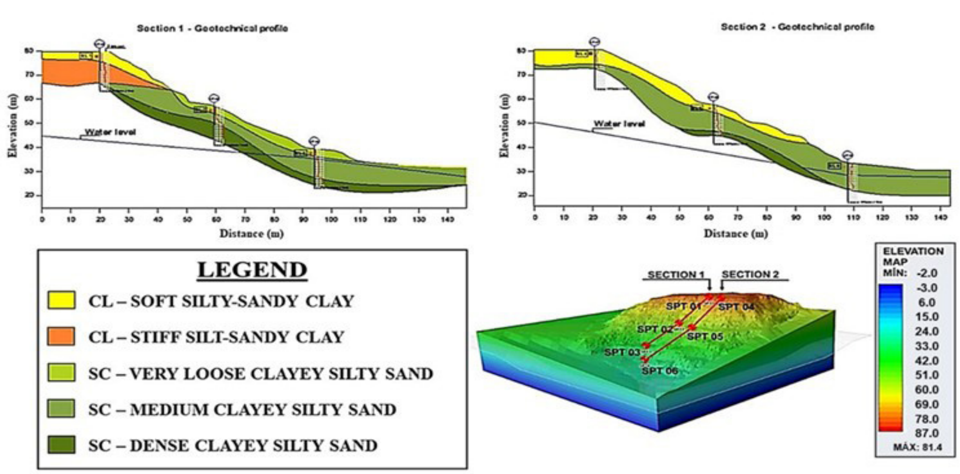

Figure 11. Geotechnical profiles obtained by interpreting SPTs and particle size analysis.

CC BY

Slide3 software (version 2019), both developed by Rocscience Inc. For the creation of the 3D model, data from the Digital Terrain Model (DTM), generated using LiDAR with a scale of 1:5000, were applied.

For the modeling of the Clayey sands (SC) soil, the following parameters were adopted: under flooded conditions, cohesion (*c'*) of 6.0 kPa and internal friction angle (ϕ') of 32º; and under natural conditions, *c* of 25 kPa and ϕ of 32º. For the Low plasticity clay (CL) soil, the parameters considered were under flooded conditions, *c'* of 5 kPa and ϕ' of 33º; and under natural conditions, *c* of 19 kPa and ϕ of 33º. The 2D stability analyses, using shear strength parameters under both natural and submerged conditions, were performed considering the following methods: Bishop, Spencer, and Morgenstern-Price (GLE). Two sections were chosen for the analysis, both passing through the sections where the SPT tests were conducted — Section 1 and Section 2. The results are presented in Table 5.

The 3D stability analyses, using shear strength parameters under both natural and submerged conditions, were performed considering the Bishop, Spencer, and Morgenstern-Price (GLE) methods. The study of the 3D stability model using the different methods (Table 6) revealed that the critical ellipsoid surfaces were located at the top of the slope, specifically between the locations where the SPT tests were conducted.

Figure 12 shows the rupture surface for the flooded condition, highlighted in black, obtained by the GLE method. The position of the cracks, highlighted in white, is also illustrated.

3.1.3.3 Conceptual synthesis

The three-dimensional analysis demonstrated good agreement between the different methods, with an average Safety Factor (*SF*) of 1.483 in the natural condition and 1.065 in the submerged condition. The safety map of the flooded condition presented includes the region where cracks and landslide blocks have appeared, indicating imminent instability.

Table 5. Results of *SF* obtained by 2D analyses - this study.

Method	Condition	Section 1	Section 2
Spencer	Natural	1.513	1.487
	Saturated	1.122	1.204
Bishop	Natural	1.538	1.488
	Saturated	1.117	1.194
GLE	Natural	1.516	1.474
	Saturated	1.114	1.190

The results highlight that, in the submerged condition, the 2D analyses in the flooded condition indicated stability ($SF \geq 1.11$). These values did not explain the signs of instability observed in the field. On the other hand, the 3D analysis, with an average *SF* of 1.065, provided a more consistent explanation for the cracks and mass movement, justifying the formation of the landslide block and suggesting that the slope reached a new condition of stability without breaking.

The discrepancies between the 2D and 3D analyses result from simplifications of the two-dimensional model, such as not considering the variation in topography, the lateral resistance of the soil and the distribution of the material domains. These simplifications lead to more conservative results.

The geotechnical investigation was considered adequate, with shear resistance parameters compatible with literature. Increased humidity and reduced suction during heavy rainfall decreased apparent cohesion, impacting safety factors in both analyses. The three-dimensional results, more accurate and realistic, better explained the stability of the slope, highlighting its effectiveness in representing the observed conditions and showing that, during heavy rains, the slope was close to breaking.

The landslide recorded on the Alto do Padre Cícero slope during the intense rainfall on May 28, 2022, confirms the results obtained from the three-dimensional analysis, which indicated that the slope was close to failure. This field-observed event corroborates the conducted analyses, reinforcing the conclusion that, under conditions of heavy rainfall, there was a real and imminent possibility of instability

3.1.4 Gravitational mass movements that occurred in May 2022

In MR-Recife, landslides result from geological conditions, human activity, relief, and precipitation (Coutinho et al., 2019). Recife and Jaboatão dos Guararapes rank 6th and 10th in Brazil in landslide-related deaths (1988–2022), with 75–85% of cases linked to rain events (Bandeira & Coutinho, 2015; Macedo & Sandre, 2022).

MR-Recife has a coastal tropical climate (As' classification), with rainfall exceeding 2,000 mm annually and an average temperature of 26.1°C. The rainy season (March–August) sees over 200 mm/month, while the dry season lasts from October to February (Coutinho et al., 2023).

The region has diverse geological units (Figure 13), with landslides occurring mainly on the Granite-Gneissic-Migmatite Complex and the Barreiras Formation, the latter

Table 6. Results of *SF* obtained by 3D analyses.

Method	Natural			Saturated		
	SF	Volume (m^3)	Max Depth (m)	*SF*	Volume (m^3)	Max Depth (m)
Bishop	1.471	1124.66	6.438	1.042	537.308	5.926
Spencer	1.483	1124.66	6.438	1.065	854.635	6.455
GLE	1.495	1565.65	6.316	1.088	537.308	5.926
Average	1.483	1271.66	6.397	1.065	643.084	6.102

CC BY

being highly susceptible due to its poorly consolidated sandy and clayey sediments (Coutinho & Severo, 2009).

A semi-detailed soil survey of Jaboatão dos Guararapes (PE), as presented by Coutinho et al. (2024), underscores the importance of incorporating pedological analyses into territorial planning. The study identified the main soil types in the region and assessed their physical and chemical properties, as well as their limitations for urban development. It revealed the predominance of poorly drained soils with high susceptibility to erosion, particularly Gleysols—characterized by a high water table and low permeability—and RED-YELLOW Argisols (PVA), which, when found on steep slopes with limited vegetation cover, are highly vulnerable to erosive processes. These findings reinforce the need to consider geotechnical and environmental risks in land-use and urban planning policies.

Between May and June 2022, disturbances associated with easterly waves triggered exceptionally intense rainfall in the states of Pernambuco, Alagoas, and Paraíba (Marengo et al., 2023). Figure 14 illustrates the accumulated precipitation

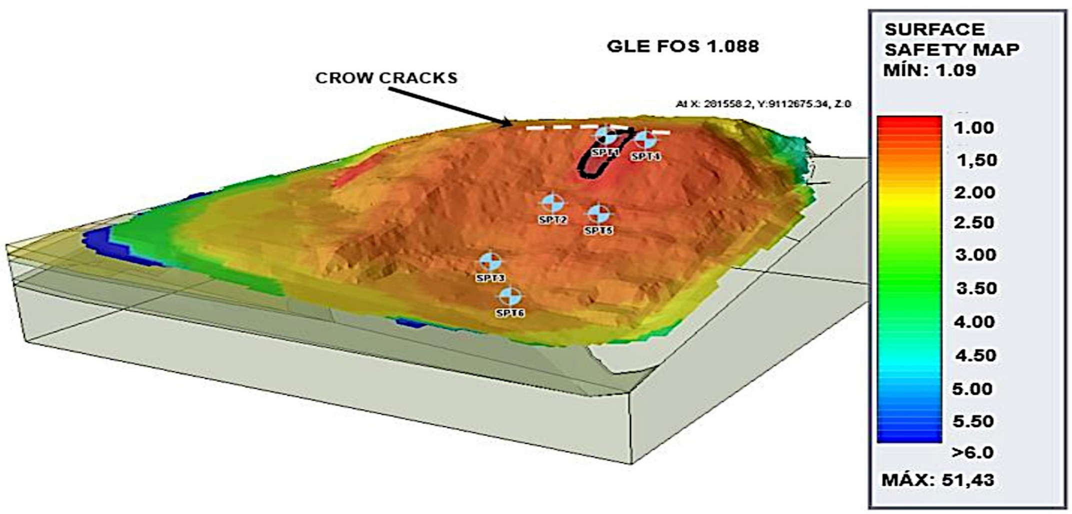

Figure 12. Surface safety map obtained by GLE's method - 3D modelling under submerged condition.

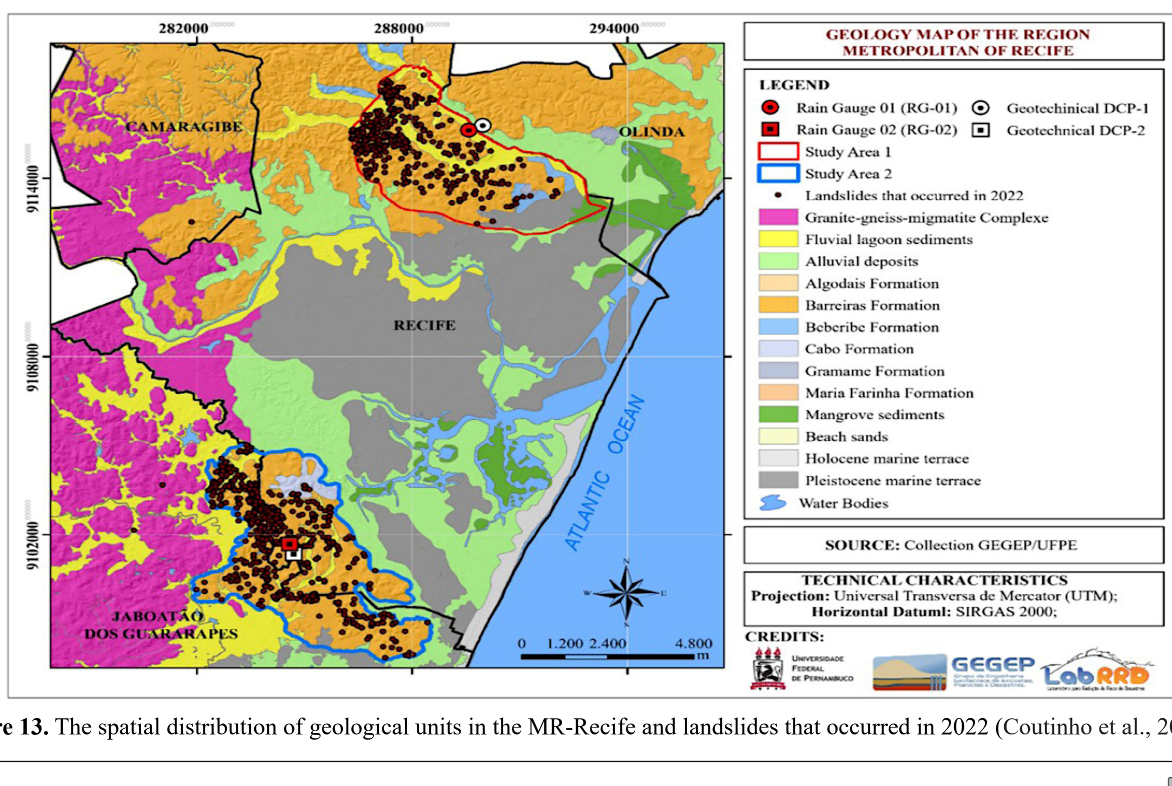

Figure 13. The spatial distribution of geological units in the MR-Recife and landslides that occurred in 2022 (Coutinho et al., 2023).

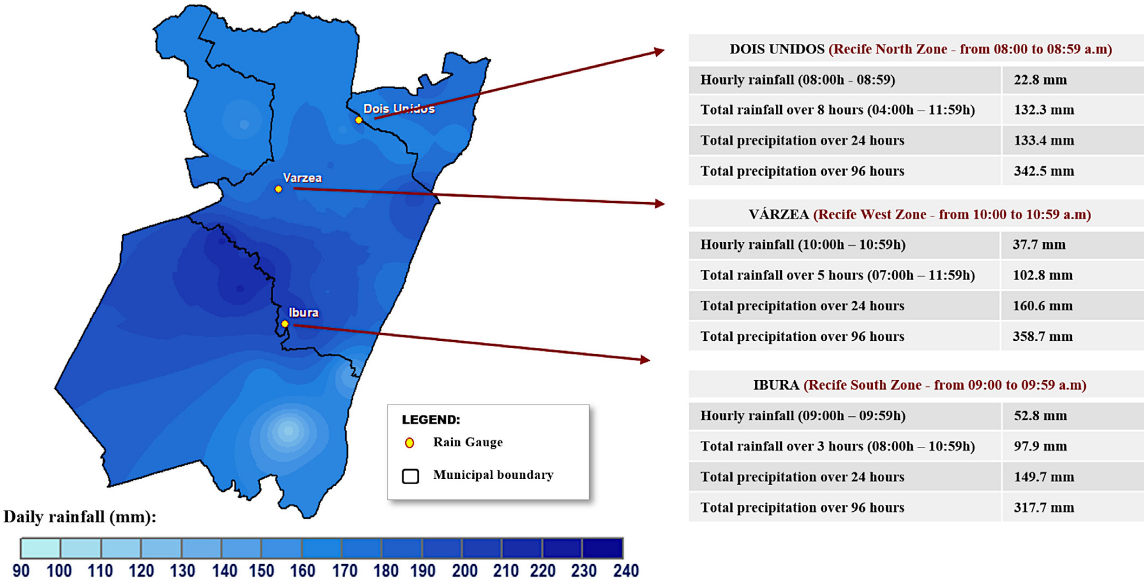

Figure 14. Distribution of accumulated precipitation in the 96 hours prior to the largest hourly rainfall event, recorded on 05/28/2022 MR-Recife (Coutinho, 2024).

volume in the 96 hours preceding May 28, 2022, when vulnerable slopes received 100 mm of rainfall in just eight hours, leading to flooding and landslides.

In preliminary studies on the 2022 event in the Metropolitan Region of Recife, Coutinho et al. (2023) investigated the hydrological soil conditions in two high-risk areas and established the foundation for an early warning system for landslides, integrating rainfall and soil moisture monitoring. The results indicate that soil moisture is highly sensitive to precipitation, with abrupt variations in response to increased hourly rainfall.

Analysis of 75 rainfall stations (Vasconcelos Junior et al., 2024) showed that the May 2022 event had an annual probability of 1 in 500 to 1 in 1000, linked to a 1.2°C rise in global temperature. While climate change increases the likelihood of extreme rainfall, a lack of comparable historical records makes precise quantification difficult.

According to Pernambuco's Executive Secretariat for Social Assistance (Recife, 2023), by July 31, 2022, the disaster had caused 133 deaths, making it the deadliest event in the state since 1975. The highest death tolls were recorded in Jaboatão dos Guararapes (64) and Recife (51), with additional fatalities in Camaragibe, Olinda, and other municipalities. Out of these deaths, 124 resulted from landslides, 8 from drowning, and 1 from electrocution.

Figure 15 illustrates the destruction in Monte Verde, Alto Santa Isabel Street (Jaboatão dos Guararapes), where four people died. The landslide displaced 140 meters of soil, reaching a final height of 1.30 meters, destroying homes and uprooting trees. Smaller subsequent landslides added to the total mobilized soil volume.

The 2022 event demonstrated that rainfall, population exposure, and infrastructure deficits were key impact factors. It highlighted the need for: Stronger links between meteorological alerts and preventive actions to mitigate risks; Climate-adaptive reconstruction incorporating stabilization and resilient infrastructure projects; Urban planning that accounts for extreme events, reducing future exposure and vulnerability. With climate change increasing extreme rainfall frequency and intensity, these measures are crucial to safeguarding MR-Recife's urban communities.

Figure 15. Ilustrative image of the landslide that occurred on 05/28/2022 on Alto Santa Isabel Street, Jaboatão dos Guararapes (Coutinho, 2024).

Ongoing research is being conducted within the framework of several projects, including CNPq 446249/2023-8 and FACEPE projects APQ-1585-3.01/22 and APQ-2290-3.01/24, coordinated by the Geotechnical Engineering Group for Disasters and Plains (GEGEP/UFPE). These studies primarily focus on the prediction of mass movements and the development of sustainable solutions for slope stabilization.

In more recent studies, published by Pereira et al. (2025), the instability mechanisms of the Joaquim Creek slope in Nova Descoberta, Northern Zone of Recife, were analyzed. The study investigated the combined effects of extreme rainfall, anthropogenic actions, surface water infiltration, pipeline leakage, and the presence of reservoirs, applying limit equilibrium methods and finite element analyses to assess the structural stability of the slope.

3.2 Case studies in the state of Rio de Janeiro

This subitem presents studies conducted on specific sections of highway BR-116, at kilometers 29 and 101, in the state of Rio de Janeiro. The analyses included geological-geotechnical investigations, instrumentation, modeling, and the application of solutions aimed at mitigating displacements (creep) in talus-colluvium deposits in the Serra do Mar.

3.2.1 Contextualization

Large colluvial deposits along the Serra do Mar escarpment, which spans southeastern Brazil (Figure 16), often have unstable slopes with a factor of safety near unity, making them prone to creep movements. This region experiences high rainfall, and mass movements typically occur during the rainy season (October to March). The study focuses on two colluvial deposits along BR-116/RJ, where pavement deformations have been recorded since the 1970s. Deep Horizontal Drains (DHDs) were installed in the colluvial deposits, and the discharge from these drains was monitored over time. Theoretical analyses were conducted to assess the impact of rainfall, Groundwater table (GWT) fluctuations, and drainage on slope stability. The study follows similar case studies in the literature (e.g. Lacerda 2004, 2007; Du et al. 2013). Geotechnical profiles were obtained using drilling and geophysical surveys, and slope monitoring was conducted with inclinometers, piezometers, and rain gauges (Ehrlich et al., 2018, 2021). Results emphasize the importance of groundwater control in maintaining slope stability and mitigating landslide risks.

3.2.2 Characteristics of the areas

3.2.2.1 Kilometer 101 of the BR-116 highway, in the state of Rio de Janeiro (RJ)

The talus-colluvium mass at km 101 varies in depth from 30 to 70 m, with a width of 200 m and length of approximately 300 m. This site has a history of slow movements, causing pavement deformations since the 1970s. Although maintenance was performed, intermittent movement continued at variable rates. Between November 2010 and November 2011, deep horizontal drains (DHDs) were installed, leading to a reduction in groundwater table (GWT) levels and movement.

The area features rugged geomorphology, with steep slopes, ridges, and peaks, including the Pedra do Sino at 2263 m in the Serra do Mar. Figure 17 shows the topography and general view around the study site. The drainage basin feeding into the site spans 7.7 km^2, with a main thalweg extending 7.4 km, and an altitude difference of 1928 m from the basin's highest point to km 101. Geologically, the study area lies at the interface of the Serra dos Orgãos and Santo Aleixo Units. The Serra dos Orgãos Unit consists of tonalitic to granitic rocks, while the Santo Aleixo Unit is made up of granodiorite with amphibolite enclaves and leucogranite intrusions (Figure 18). These formations are part of the Brasilian Orogeny, dating from 630 to 480 Ma.

Homogeneous plutons, sometimes zoned with evidence of magma mingling and mixing, are observed. Late aplitic

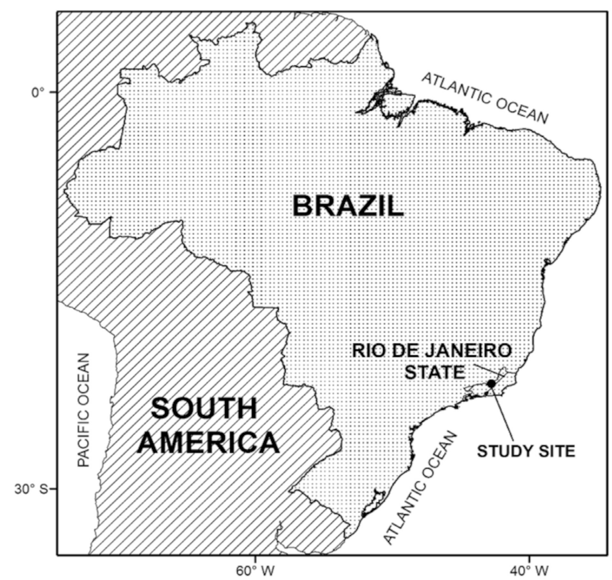

Figure 16. Location of the study site in Brazil.

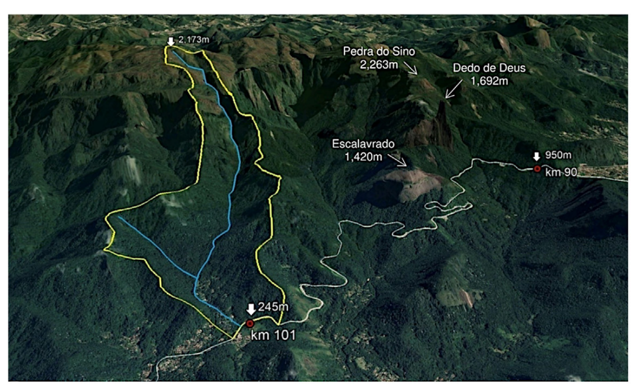

Figure 17. Topography and general view around the study site (BR-116/RJ km 101).

CC BY

phases are widespread. According to the geological section of the area (Figure 19), the terrain has, as a regional setting, a granite substrate located above the Santo Aleixo Unit, mostly composed of gneiss. The region shows tectonic patterns with significant erosion, including translational and rotational slides, often along soil-rock interfaces. Water pressure, especially during rainy periods, plays a key role in slope instability, contributing to the reactivation of colluvium deposits, which can show creeping movements.

3.2.2.2 Kilometer 116 of the BR-116 highway, in the state of Rio de Janeiro (RJ)

The colluvial deposit under consideration is located near the border of the states of Rio de Janeiro and Minas Gerais. Figure 20 presents a general view of the location, and Figure 21 shows the topography around the site. In the area, convex-concave hills with rounded or pointed tops are observed, with the presence of colluvium, alluvium and, subordinately, deposits of talus. There is a prevalence of topographic amplitudes between 200 and 400 m and medium gradients, with the presence of prominent residual forms and elevated gradients. The drainage density of the region is from middle to high.

Figure 22 shows a geological map of the region. The deposit occurs in an area of shear zone and granite-gneiss rocks, with persistent parallel fractures that dip favorable to the groundwater flow in the direction of the slope. Figure 23 illustrates the longitudinal profile, indicated in Figure 21. Besides direct rainfall infiltration in the colluvium, the presence of upper terraces with watercourses and alluvial plains may lead to rainfall accumulation that may infiltrate through permeable fractures in the rock below and reach the colluvium deposit downslope.

3.2.3 Results and discussion

3.2.3.1 Kilometer 101 of the BR-116 highway, in the state of Rio de Janeiro (RJ)

Geophysical surveys and rotary drill samples from km 101 of BR-116/RJ reveal a talus-colluvium deposit. At km 101, rock blocks and soil from the Santo Aleixo Unit have accumulated over time in a thalweg, with a talus-colluvium deposit stretching about 300 m, with depths varying between 30 and 70 m. Four boreholes, drilled to a depth of 54 m, encountered medium-dense yellowish-brown silty sand ($7 < N_{SPT} < 39$) up to 9 m, and weathered granite interspersed with soil from 9 to 54 m.

The characterization of soil samples taken from 2 m below the surface indicate 37% water content, 93% saturation, and a void ratio of 1.07, with specific gravity (*GS*) of 2.68. Atterberg limits indicated *LL* (Liquid Limit) and *PL* (Plastic Limit) equal to 38% and 48%, respectively. The unit weight was 17 kN/m^3 natural and 18 kN/m^3 saturated. Direct shear tests under submerged conditions revealed a cohesive intercept of 25 kPa and an effective friction angle of 35°. To reduce

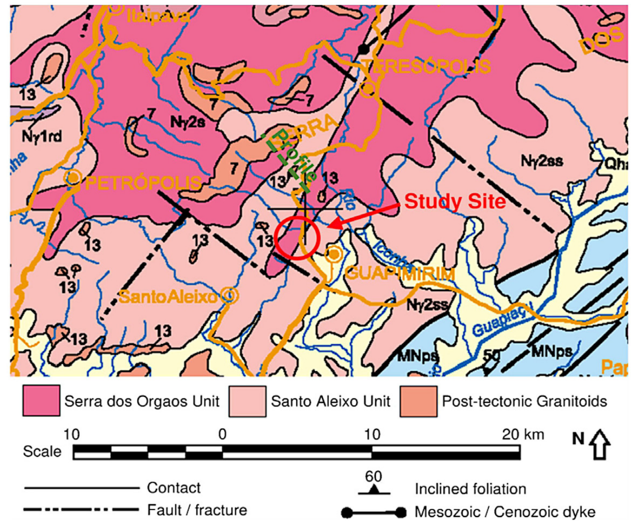

Figure 18. Geological map of the region (CPRM, 2000).

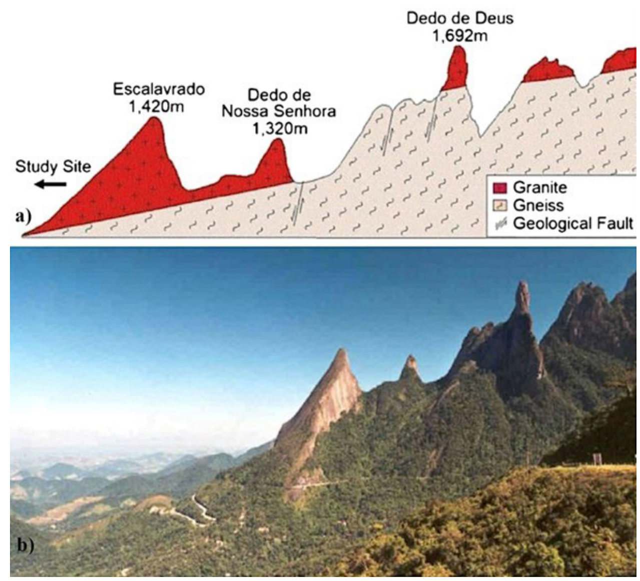

Figure 19. Schematic geological profile (Junho & Penha, 1982) (a) and general view (b) of the Serra dos Orgãos.

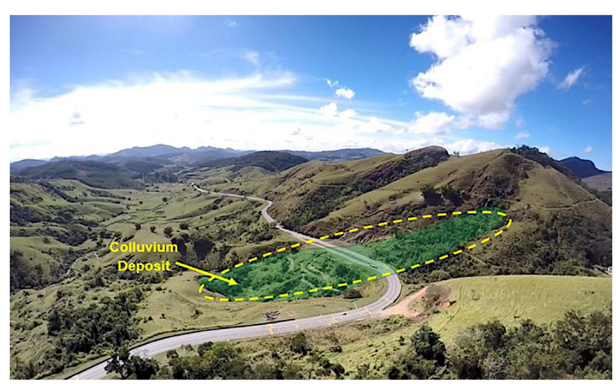

Figure 20. General view of the area and the colluvium deposit under analysis (BR-116/RJ km 29).

CC BY

groundwater table (GWT) levels and pore water pressure in the colluvium, 50 deep horizontal drains (DHDs) were installed from November 2010 to November 2011, extending up to 50 m with a 15° upward inclination (Figure 24).

Rainfall was measured at stations located at km 92, 94, and 105. Inclinometers I1 and I2, installed in 2007, showed significant lateral displacements, with failure surfaces identified at 10 m depth for I1 and 18 m for I2 (Figure 25). Over 13 years of monitoring, both inclinometers recorded 140 mm of displacement, with a decrease in lateral movement after DHDs were installed. The installation of DHDs led to prolonged lower GWT levels, reducing lateral displacements (Figure 26). The Morgenstern-Price method was applied to assess the factor of safety (*SF*) for potential failure mechanisms. For rotational failure, *SF* was 1.13, while for translational failure, *SF* values were 1.12 and 1.06 for sections A and B, respectively. The overall *SF* for the colluvium mass was 1.08. As the GWT lowered due to DHDs, the *SF* improved. Between 2017 and 2018, there was no cleaning of the DHDs. As a result, a reduction in the *SF* was observed. After the DHDs were cleaned, the *SF* value increased again, remaining close to 1.5. This observed behavior calls attention to the importance of drain maintenance.

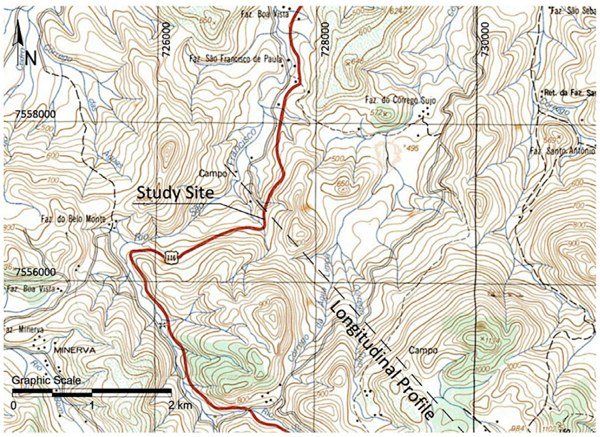

Figure 21. Topography around the study site.

3.2.3.2 Kilometer 116 of the BR-116 highway, in the state of Rio de Janeiro (RJ)

Geophysical and drilling data at km 29 revealed a colluvium-filled paleo-thalweg with an average slope of 19° and 450 m in length, similar to the deposit at km 101. The colluvium sits atop a 5-m-thick residual soil layer, followed by granite-gneiss with oxidized fractures dipping at 30°, which is unfavorable for slope stability. The soil characterization data from km 29, present 11% water content, 35% saturation, and a void ratio of 0.83, with *GS* of 2.73. The unit weight was 17 kN/m^3 natural and 20 kN/m^3 saturated. The tests indicated that the soil is non-plastic. The direct shear tests revealed an effective friction angle of 29° with no cohesive intercept.

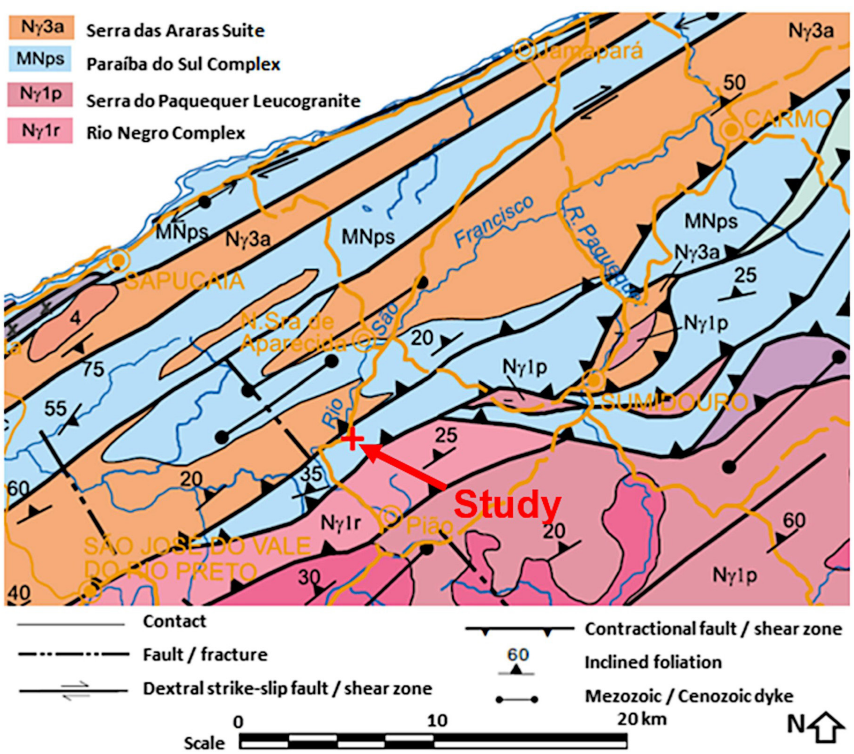

Figure 22. Geological map indicating the shear zones observed in the region (CPRM, 2000).

CC BY

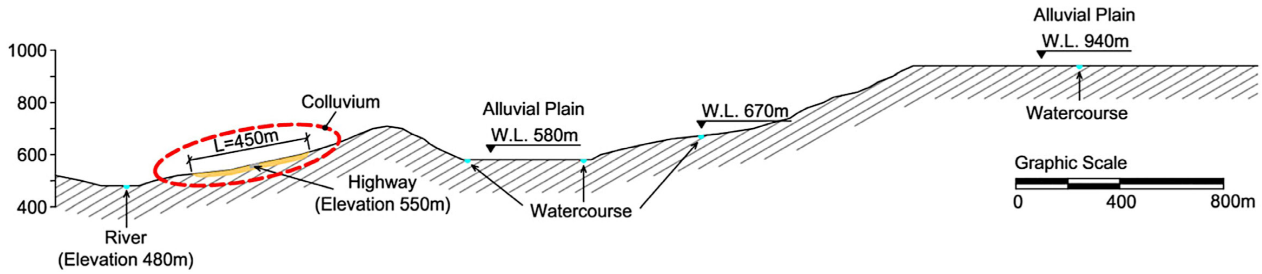

Figure 23. Longitudinal profile showing the presence of upper terraces with watercourses and alluvial plains.

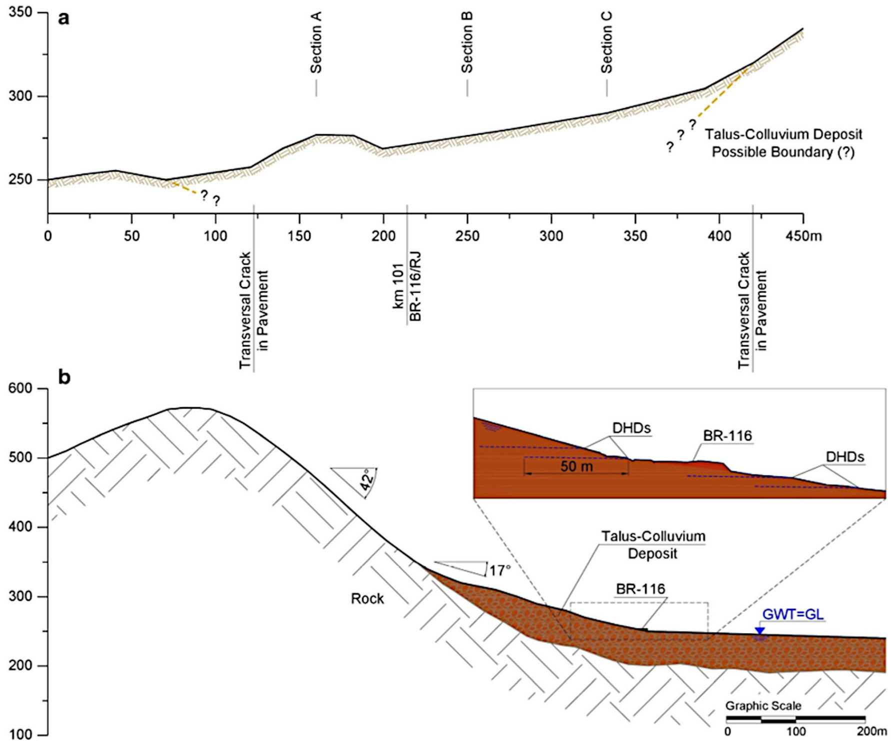

Figure 24. The talus-colluvium deposit: (a) longitudinal alignment and; (b) cross section B.

Lateral displacements were monitored with inclinometers I1 and I2, and the results from May 2013 to March 2016 show trends in displacement (Figure 27 and Figure 28). The region has significant groundwater recharge sources, including upper terraces with alluvial deposits and watercourses that influence groundwater flow and slope stability. To manage GWT and pore water pressures, DHDs were installed in 2015, extending up to 100 m (Figure 28). Water level measurements indicated fluctuating artesian pressures before the DHDs were installed in 2015.

Post-installation, piezometer and water level readings stabilized around 18 m, though rainfall still influenced GWT (Figure 29). Significant GWT increases were noted during heavy rainfall in December 2015, possibly due to regional recharge sources. The DHDs effectively lowered GWT levels, as shown by the decrease in piezometric levels after installation. Lateral displacement measurements, shown in Figure 30, were compared to 25-day accumulated rainfall data. Displacements were higher when rainfall exceeded 250 mm over 25 days. However, the DHDs helped maintain lower GWT levels, reducing displacements in 2015 and 2016 compared to 2012 and 2014. This demonstrates the effectiveness of DHDs in stabilizing colluvium deposits.

3.2.4 Conceptual synthesis

In both km 101 and km 29 of BR-116/RJ, the installation of DHDs significantly contributed to the stabilization of

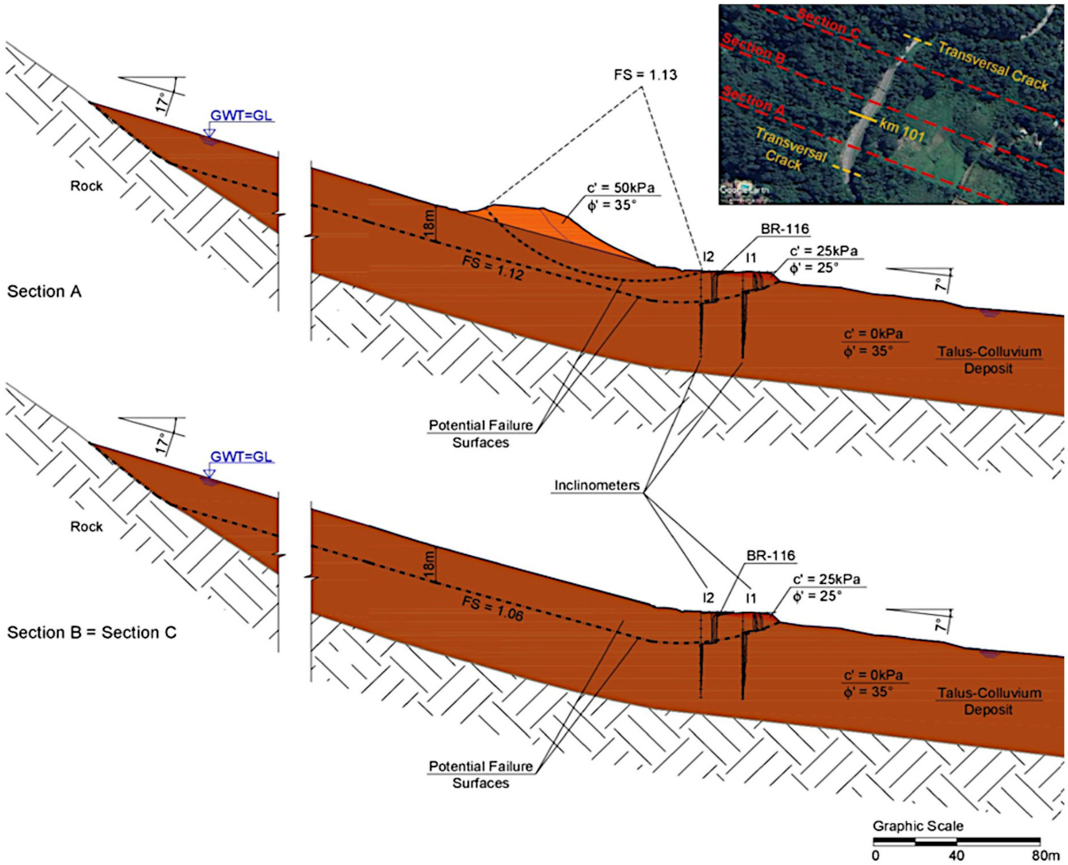

Figure 25. Factor of safety values for different potential failure surfaces.

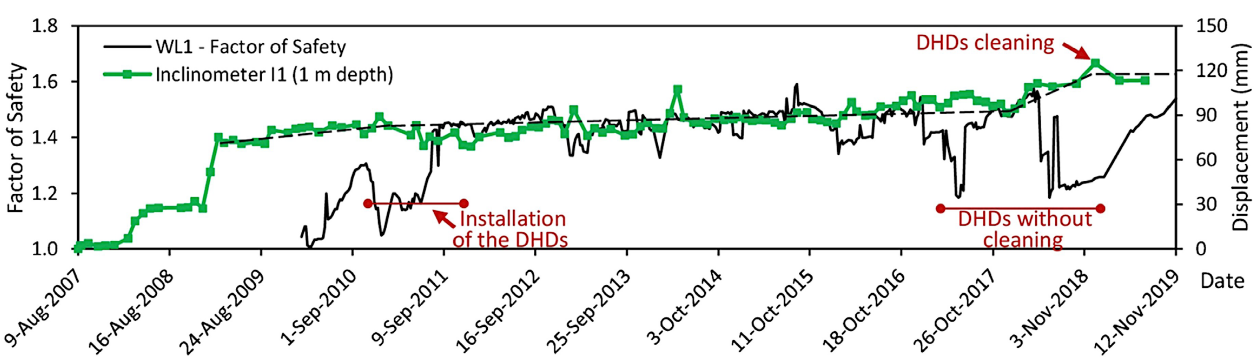

Figure 26. Displacements versus factor of safety (based on WL1 measurements).

colluvial deposits by lowering GWT levels and reducing lateral displacements. The monitoring results confirm that DHDs are an effective measure for managing pore water pressures in colluvium deposits, improving slope stability, and preventing failure. Regular maintenance of these drainage systems is crucial to maintaining their effectiveness in long-term slope stabilization. The correlation between rainfall and displacements further underscores the importance of managing groundwater levels to minimize slope movement. Moreover, inclinometer readings indicate that, before the installation of the DHDs, in both locations (BR 116/RJ km 101 and km 29) the movement in the slope

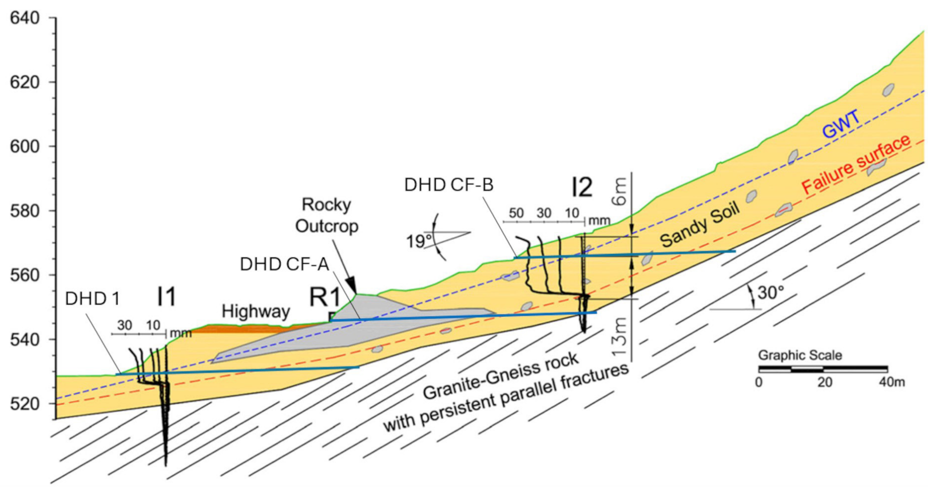

Figure 27. Geological-geotechnical profile of the rocky outcrop area with the schematic representation of the rock fractures and measurements and location of the inclinometers (I1 and I2), the position of the surface measuring mark (R1) at the rocky outcrop section and deep horizontal drains (DHD 1, DHD CF-A, and DHD CFB).

would increase when the 25-day accumulated rainfall exceeded 250 mm.

3.3 Case studies in the state of São Paulo

This subitem discusses studies conducted on urbanized slopes in the city of São Paulo. The analyses included geological-geotechnical investigations, instrumentation, and modeling, with the aim of identifying the variables that most influence stability and, subsequently, proposing stabilization solutions.

3.3.1 The effect of unsaturated conditions on slope stability

Franch & Futai (2009) conducted an experimental study on a slope in São Paulo, divided into two sections with contrasting surface coverage: one portion was vegetated, and the other was covered with a thin mortar layer. This setup allowed for an in-depth analysis of how surface treatments affect infiltration and suction dynamics. The vegetated area exhibited significant reductions in pore-water pressure during dry periods, a result of evapotranspiration processes. Conversely, the mortar-covered section restricted rainwater infiltration, leading to higher suction levels during rainy periods. Figure 31 from the study shows the experimental field with mortar and vegetation coverage, illustrating the contrasting infiltration dynamics. These findings underscore the importance of selecting appropriate surface treatments based on slope conditions and stabilization goals.

Building on this work, Franch & Futai (2010) expanded their investigation to analyze seasonal variations in pore-water pressure over an eight-month period. Their study utilized tensiometers to monitor daily changes in water

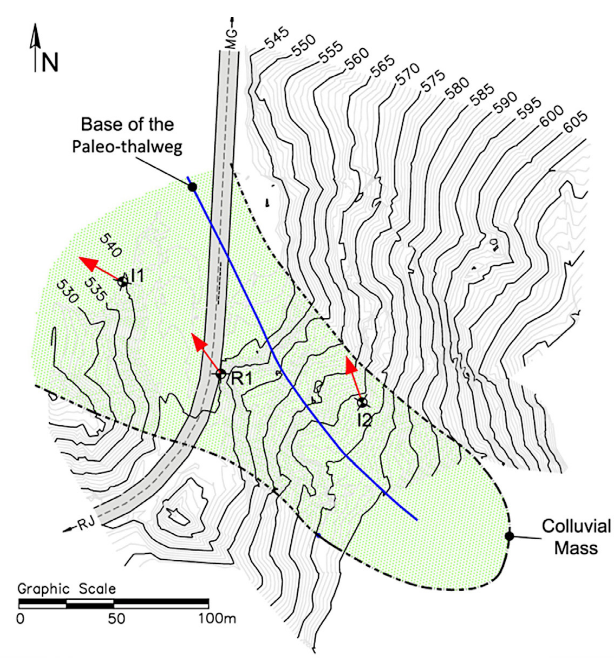

Figure 28. Topographic map of the area with delimitation of the colluvial deposit defined by the geophysical survey and indication of the direction of lateral displacements (red arrows) measured by inclinometer I1 and I2 and by topographic readings at mark R1.

pressure, precipitation, and groundwater levels. The results revealed distinct hydrological behaviors in clayey and silty soils. During rainy periods, the clayey layer exhibited rapid increases in pore-water pressure, sometimes leading to the formation of suspended water tables near the slope's crest. This phenomenon was attributed to the low permeability

CC BY

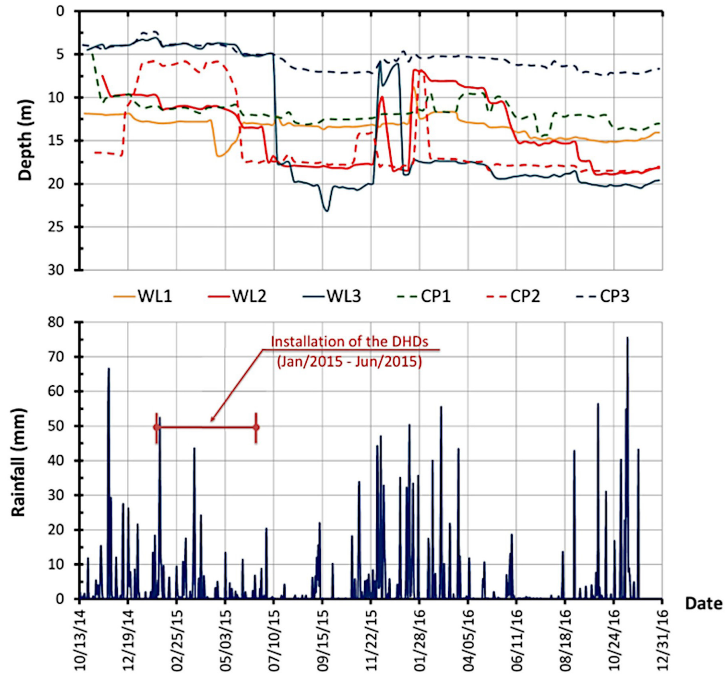

Figure 29. Piezometric and water table levels plotted against 24-h accumulated rainfall measured at Rain gauge Station 1 (km 23).

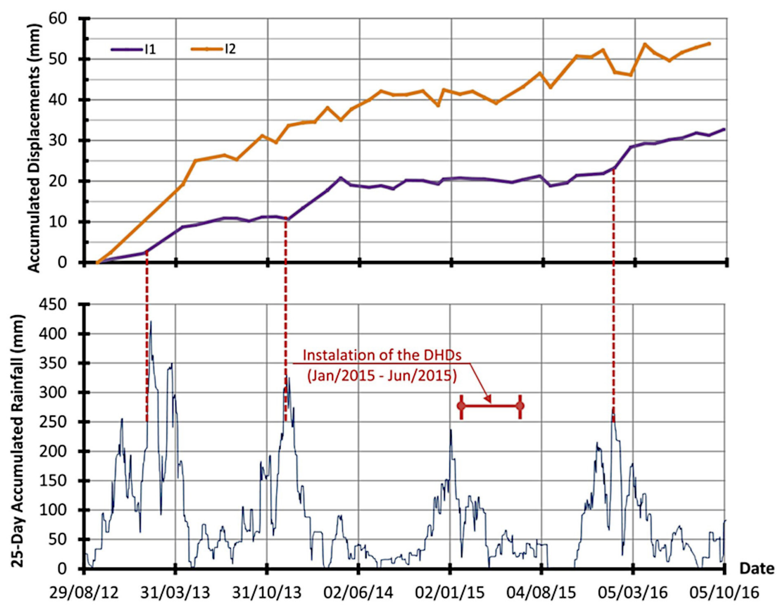

Figure 30. Horizontal displacements measured by inclinometers I1 and I2 versus 25-day accumulated rainfall measured at Rain gauge Station 2 (km 40).

and anisotropic characteristics of the clay. Figure 32 from their findings shows the water pressure distribution during a rainy season, highlighting the critical zones of potential instability. Stability analyses conducted during this period showed a 7% decrease in the safety factor, emphasizing the critical impact of seasonal changes on slope stability. Dry periods, on the other hand, saw a gradual recovery of suction levels, particularly in vegetated areas, where evapotranspiration played a significant role in stabilizing the slope.

3.3.2 Seasonal water pressure variations and creep behavior in the city of São Paulo

Godois et al. (2009) extended the investigation of creeping slopes by analyzing the Vila Albertina slope in São Paulo. This site features an 80,000 m^2 unstable mass that has been in motion for decades due to anthropogenic activities and hydrological influences. Historical aerial imagery and field data, including inclinometer readings and piezometric measurements, were used to delineate the extent of the unstable area.

Figure 31. Experimental field - panoramic view (Franch & Futai, 2009).

During monitoring, significant correlations between rainfall, water table fluctuations, and displacement rates were observed. Figure 33 illustrates the geotechnical profile of the slope, showing the perched water table and the low-permeability soil layers contributing to the creeping behavior. Figure 34 highlights superficial displacement readings over time, demonstrating the impact of seasonal rainfall on slope displacements.

Stabilization efforts, including horizontal drains and retaining structures, mitigated movement in some areas. However, residual risks persist due to the complexity of the site's hydrological conditions. These findings highlight the need for adaptive management and ongoing monitoring to address the evolving dynamics of colluvial creep.

3.3.3 Conceptual synthesis

The reviewed studies collectively underscore the complex interplay between hydrology, soil mechanics, and geomorphology in driving creep movements in colluvial masses. Key mechanisms include:

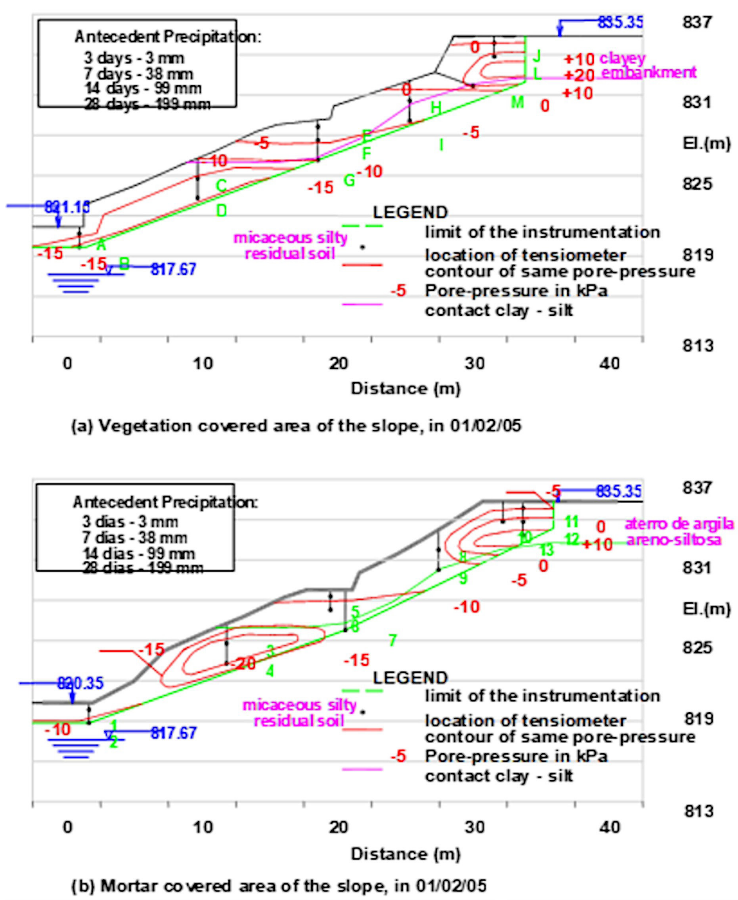

Figure 32. Pore-water pressure distribution in the slope, on February 1st: (a) in vegetation and (b) mortar covered parts of the slope.

CC BY

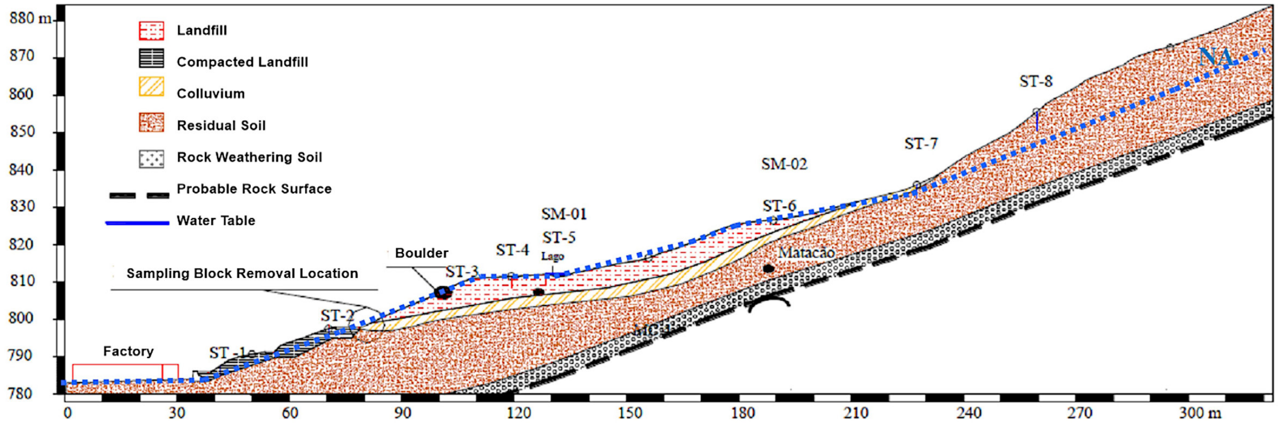

Figure 33. Geotechnical profile of the slope.

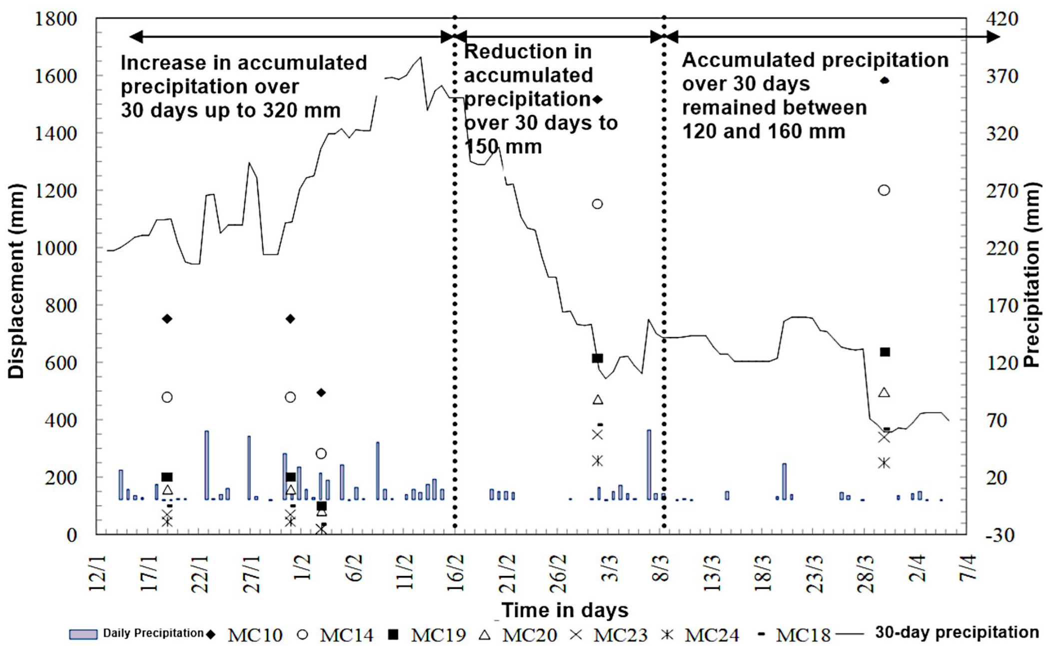

Figure 34. Displacements of the 30-day cumulative rainfall marker over time.

- **Rainfall Infiltration**: Intense and prolonged rainfall events are primary drivers of increased pore-water pressure, reducing shear strength and accelerating creep movements.
- **Perched Water Tables**: The formation of localized water tables within low-permeability layers exacerbates instability by concentrating pore pressures in critical zones.
- **Seasonal Variations**: The cyclic nature of rainfall and evapotranspiration leads to alternating phases of suction recovery and pressure buildup, influencing the rate and extent of displacement.

The findings from these studies offer several implications for geotechnical engineering and slope management:

- **Instrumentation and Monitoring**: Comprehensive monitoring systems, including inclinometers and piezometers, are essential for capturing the temporal and spatial dynamics of creep movements.
- **Drainage Solutions**: Effective drainage measures, such as sub-horizontal drains, can mitigate the formation of perched water tables and reduce pore-water pressures.
- **Numerical Modeling**: Tools like SEEP/W provide critical insights into the interactions between hydraulic

processes and slope stability, enabling proactive risk management.

By integrating these approaches, engineers can develop tailored solutions to address the unique challenges posed by saturated colluvial masses, ensuring the safety and resilience of critical infrastructure.

Creep movements in saturated colluvial masses are governed by a complex interplay of hydrological and geotechnical factors. The studies reviewed in this subitem highlight the critical role of rainfall infiltration, pore-water pressure dynamics, and soil properties in shaping the behavior of these slopes. Through detailed field monitoring and numerical simulations, researchers have provided valuable insights into the mechanisms driving creep and the strategies needed to mitigate its impacts. Future work should focus on advancing monitoring technologies and refining predictive models to enhance our understanding and management of these persistent geotechnical challenges.

3.4 Case studies in the state of Paraná

This subitem presents the efforts made to understand and stabilize colluvium deposits in the Serra do Mar, which posed risks to the OLAPA pipeline, located in the state of Paraná, due to displacements caused by creep.

3.4.1 Experimental study on the behavior of saturated colluvial masses affecting pipelines

The stability of saturated colluvial masses presents significant challenges to geotechnical engineers, especially when these masses interact with critical infrastructure such as buried pipelines. This nested item focuses on the OLAPA oil pipeline case in Serra do Mar, Paraná, Brazil, studied by Suzuki et al. (2013). The study highlights the impact of cumulative rainfall, hydrological conditions, and stabilization measures on the displacement of colluvial masses and their implications for infrastructure integrity.

The OLAPA pipeline, operational since 1977, stretches 94 kilometers, connecting the REPAR refinery to the TEPAR terminal. A key segment of the pipeline, located at km 57+200, crosses a colluvial tongue in the Serra do Mar region. In March 1999, longitudinal and transverse cracks were detected near the pipeline axis, indicating hillside creep. These movements, driven by the perched water table and intense rainfall, posed a significant risk to pipeline integrity (Suzuki et al., 2013).

3.4.1.1 Geotechnical investigation and instrumentation

A geotechnical investigation program was implemented, including boreholes for subsoil reconnaissance and installation of monitoring instruments. The instrumentation consisted of inclinometers, piezometers, and pluviometers. Initial readings in October 2000 confirmed slow displacement of the hillside. However, following heavy rainfall in February 2001, an acceleration in movement occurred, resulting in pipeline rupture. The geotechnical profile comprised saturated silty clay colluvium, 11 to 21 meters thick, overlying sandy silt residual soil and altered migmatite rock.

Instrumentation data revealed strong correlations between cumulative rainfall and displacement rates. Movements accelerated when 25-day cumulative rainfall exceeded 250 mm. Figure 35 illustrates the displacement profiles of inclinometer

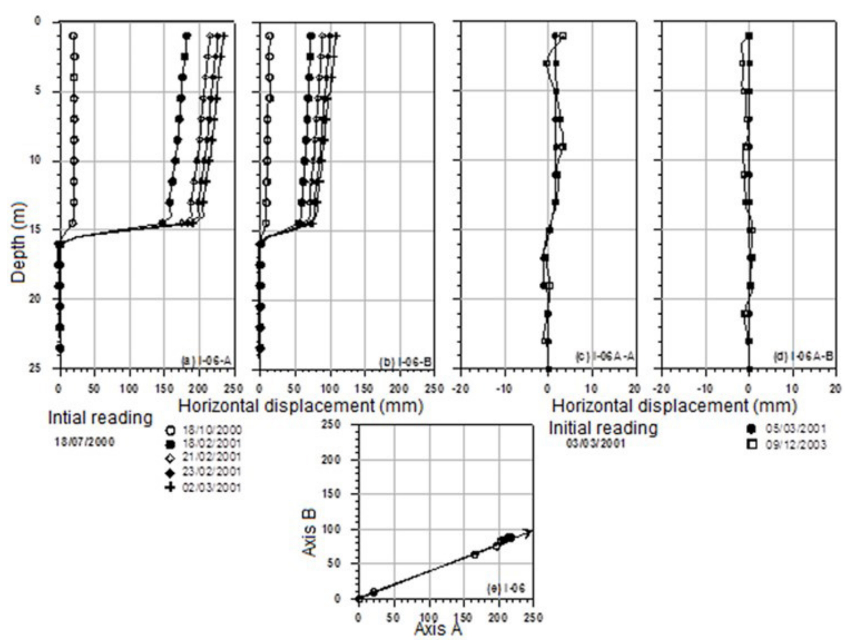

Figure 35. Measurements of the inclinometer I-06 and I-06 A (Suzuki et al., 2013).

CC BY

I-06, which recorded 20 mm of movement in October 2000 and 180 mm following the February 2001 rainfall. Excessive deformations rendered the inclinometer unusable, leading to its replacement with I-06A in March 2001 (Suzuki et al., 2013). The profile along the axis of the colluvium showed inclinometer measurements very coherent, as shown in Figure 36.

Figure 37 shows the correlation between rainfall intensity, inclinometer displacements, and piezometric elevations. Peaks in displacement coincided with elevated piezometric levels, emphasizing the role of pore-water pressures in driving hillside movements.

3.4.1.2 Stabilization measures

Stabilization efforts focused on managing groundwater through surface drainage and deep sub-horizontal drains (DHD). The first phase of stabilization, completed in March 2001, included the installation of 56 DHDs across eight series. Piezometer readings confirmed the effectiveness of these measures, with significant reductions in pore-water pressures and stabilization of hillside movements (Suzuki et al., 2013).

The post-stabilization displacement profiles of inclinometer I-06A, which showed negligible movements over three years of monitoring. These results highlight the critical role of drainage in mitigating risks associated with saturated colluvial masses.

3.4.1.3 Discussion

The OLAPA case study underscores the complexity of managing infrastructure in geologically active regions. The perched water table, combined with the low-permeability clayey soils, created conditions conducive to significant hillside movements during periods of intense rainfall. The monitoring program provided essential data for correlating rainfall, piezometric levels, and displacements, enabling timely stabilization interventions.

The success of stabilization measures, particularly deep sub-horizontal drains, demonstrates their efficacy in reducing pore-water pressures and preventing further displacement. This case also highlights the importance of comprehensive geotechnical investigations and long-term monitoring in designing effective stabilization strategies for slopes intersected by critical infrastructure.

3.4.1.4 Conceptual synthesis

The OLAPA pipeline case provides valuable insights into the behavior of saturated colluvial masses and the measures necessary to mitigate associated risks. Key findings include:

1. Strong correlations between cumulative rainfall and hillside displacement emphasize the need for continuous hydrological monitoring.
2. Deep sub-horizontal drains effectively reduced pore-water pressures and stabilized hillside movements.
3. Comprehensive instrumentation programs are essential for understanding slope dynamics and guiding stabilization efforts.

Future research should explore the long-term performance of stabilization measures under varying climatic conditions and their broader applicability to similar geotechnical challenges.

3.5 Case studies in the state of Rio Grande do Sul

This subitem presents the methodology used to understand the gravitational mass movement recorded near São Vendelino (RS). The study included geological-geotechnical investigations and instrumentation, as well as the application of numerical simulations to analyze the infiltration process and calculate the safety factor. Lastly, a brief overview of the magnitude and impacts of the event that occurred in the state in May 2024 is provided.

3.5.1 Back-analysis of landslide in São Vendelino (RS) using the infinite slope technique

This study presents findings from 18 months of field tests, laboratory analyses, and monitoring of precipitation and pore pressure. Flow analyses and back-analysis were performed on a slope affected by rapid translational landslides during torrential rainfall (~148 mm/2h) in December 2000,

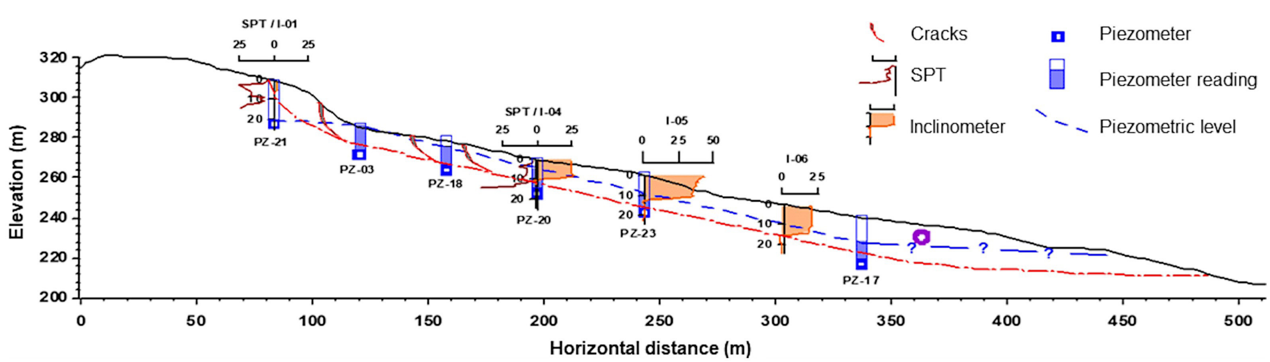

Figure 36. Section AA along the colluvium axis shown the movements detected by the inclinometers (Suzuki et al., 2012).

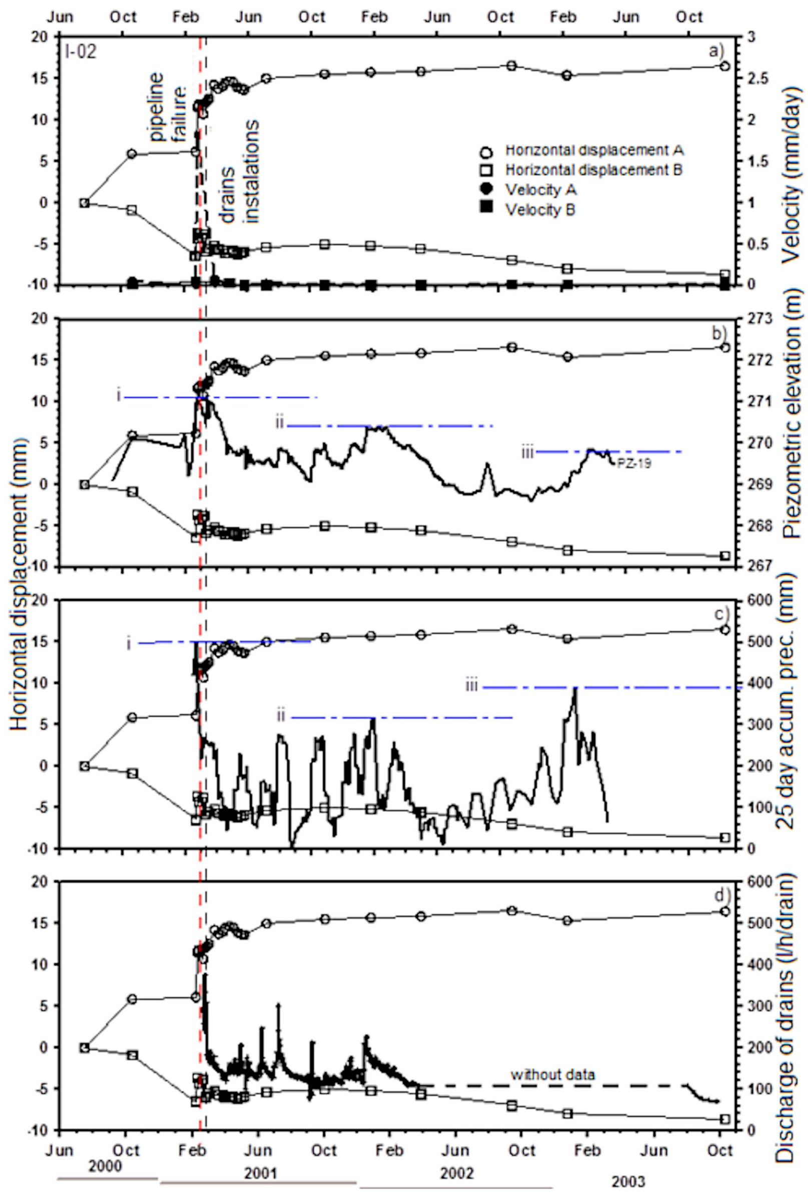

Figure 37. Correlation between inclinometer I-02, piezometer PZ-19, accumulated precipitation 25 days and rate flow drains.

São Vendelino/RS. Flow analysis using failure-period rainfall data correlated well with observed failures.

The study area, located along RS-122 (km 45+340 to 45+380), spans Alto Feliz, Carlos Barbosa, and São Vendelino (RS), where dozens of mass movements and debris flows occurred (Azambuja et al., 2001). This mountainous region features relief shaped by local fractures, with humid climate conditions intensifying fluvial dissection and chemical weathering, creating concave-convex slopes and stepped terraces.

At higher elevations, basalts and rhyodacites dominate. Basaltic flows are typically ≤15 m thick, while acidic top flows can reach 60 m. The region's three main tectonic lineaments (N30E, N70E, N60W) influence relief and drainage patterns (Azambuja et al., 2001).

Field observations in 2005 revealed the elongated, narrow scar (1–2.5 m width) left by the 2000 debris flow. The scar bottom featured thin soil deposits or exposed rock, while its lateral edges consisted of heterogeneous colluvial soils with a silt-clay matrix and basaltic blocks (Bressani et al., 2006).

3.5.1.1 Geological-geotechnical investigation

For the development of the experimental work, samples were collected at two distinct points of the studied slope. The samples were named according to the elevations from which

CC BY

they were extracted: i) Sample 351: colluvium adjacent to the scar; ii) Sample 360 m: colluvium located near the upper limit of the scar. Table 7 presents a summary of the results from the characterization tests performed. The average degree of saturation obtained was 67%, and the void ratio ranged between 1.26 and 1.56. The results from the granulometry tests with dispersing agent indicated a predominance of clay and silt (Table 8).

To determine the hydraulic conductivity in the field, tests were conducted using Casagrande piezometers (Silveira, 2008; Bressani et al., 2006). Two piezometers were installed in boreholes made with an auger at different elevations of the studied slope for conducting the tests. The details of the procedures were described by Bressani et al. (2006). Variable and constant head tests were performed on these piezometers. Table 9 presents the main results obtained from the tests.

Hydraulic conductivity tests were also conducted in the laboratory using undisturbed and remolded sample specimens. The tests were performed on three undisturbed specimens, subjected to different effective confining stresses. Additionally, a test was conducted with one remolded specimen. The undisturbed specimens were labeled CHgi-1, CHgi-2, and CHgi-3, while the remolded specimen was labeled CHgr-1. The tests were conducted using a mercury column apparatus described by Bjerrum & Huder (1957).

The specimen CHgi-1 was tested under an effective confining stress of 75 kPa. The specimen CHgi-2 was tested under two levels of effective confining stress (50 and 80 kPa). The specimens CHgi-3 and CHgr-1 (remolded) were tested under four levels of effective confining stress (40, 70, 100, and 200 kPa). The values of the hydraulic gradient in the tests ranged from i = 9.3 to i = 9.5. The water volume percolated through each sample was approximately 3 cm^3.

Table 7. Unit weight and plasticity index.

Soil (m)	γ_s (kN/m^3)	*LL* (%)	*PI* (%)
351	28.27	60.4	18.2
360	28.91	55.9	15.9

Table 8. Soil granulometry.

Soil (m)	% clay	% silt	% sand	% coarse
351	41	41.5	15.5	2.0
360	40	45	13.5	1.5

Table 9. Piezometer results.

Elevation (test type)	z (cm)	L (cm)	H_1 (cm)	H_2 (cm)	K_{sat} (cm/s)
347(var)	105	35	150.5	122	1.8x10^{-2}
361(var)	95	21	127.5	99	5.9x10^{-3}
347(cte)	105	35	90		1.3x10^{-2}

The results obtained for the undisturbed and remolded samples showed very similar variations regarding the effective confining stresses. The results highlighted a clear influence of the effective confining stresses on the hydraulic conductivity coefficient, with a reduction of approximately 10 times within the analyzed stress range. This indicates that the increase in stresses affects the soil structure, reducing macropores, which are responsible for a large part of the water flow.

Although the colluvial soil is classified as silty clay, it showed hydraulic conductivities in the same order of magnitude as typical sandy soils. The difference between the results obtained for the remolded sample (CHgr-1) and the undisturbed sample (CHgi-3) was not significant. The variation of the hydraulic conductivity coefficient with effective confining stress is presented in Figure 38 (average values). The value K_{sat} = 3 x 10^{-3} cm/s was adopted as representative of the field soil.

Triaxial tests were conducted with effective confining stresses ranging from 30 to 200 kPa on both undisturbed and remolded samples. The tests followed conventional and special effective stress paths, such as CD, CU, CID-U, and CSD (constant shear drained). The testing rate was 0.045 mm/min for undrained tests and 0.005 mm/min for drained tests. Table 10 presents a summary of the shear strength parameters obtained. The shear strength parameters showed significant variation depending on the stress level and the soil's molding condition (intact or remolded). There was a noticeable small variation in the shear strength parameters obtained in the different tests, with characteristic values of c' = 7.2-13.9 kPa e ϕ' = 31.6º.

3.5.1.2 Monitoring

Electrical transducers were installed in four Casagrande piezometers to monitor pore pressures in the field, with readings

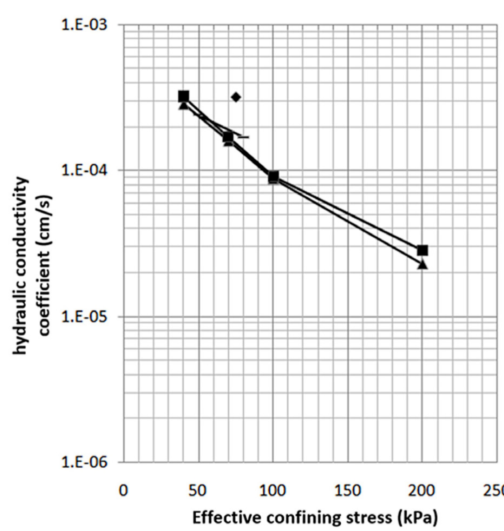

Figure 38. Hydraulic coefficient of conductivity versus effective confining stress.

CC BY

recorded every 30 minutes and collected every 2 months. An automatic rain gauge was also installed on the hillside, which recorded a maximum rainfall of 20 mm/h in one hour (November 14th, 2007). Despite this, pore pressure measurements remained below 1 kPa during the 20-month monitoring period (June/06 to February/08). The transducers were calibrated every 6 months, without showing significant differences.

3.5.1.3 Flow analysis

Numerical flow analyses were performed using Seep/W software to study the variation of pore pressure in the colluvial soil layer of the slope as a function of precipitation. The geotechnical profile, presented in Figure 39, was defined based on the geometry, geology, and hydraulic conductivity of the slope, considering a 2.0 m soil layer over the impermeable rock. The adopted saturated hydraulic conductivity was 3.0 x 10^{-3} cm/s, based on experimental tests. Unsaturated conductivity was estimated using the characteristic curve and the model of Fredlund et al. (1994). The simulation used a precipitation rate of 75 mm/h for 2 hours.

Figure 40 presents the rise of the groundwater level over time in relation to the soil-rock contact at three positions: elevations of 351 m, 359 m and 366 m. The increase in pore pressures at the base of the soil was only observed after 40 minutes, with a more pronounced increase in areas with steeper slopes. This increase in pore pressure was most pronounced at elevation 359 m, where the slope is steeper.

3.5.1.4 Stability analysis

Based on the experimental data obtained in the described program, slope stability analyses were performed. The shear strength parameters used in the analyses varied between those obtained in drained triaxial tests with reshaped and undeformed specimens (c' = 7.2 - 13.9 kPa e ϕ' = 31.6º).

The conventional stability analyses indicated that the critical failure surfaces were restricted to the top of the scar observed in the field. However, the three-dimensional effects due to the small width of the failure are unknown. Therefore, for simplification, only the analyses conducted using the infinite slope method (2D) with parallel flow (Equation 1) are presented.

$$SF = \frac{c' + \left(\gamma_t - m.\gamma_w\right).z.\cos^2\beta.tg\varphi'}{\gamma_t.z.sen\beta.\cos\beta} \quad (1)$$

With experimental data, these simplified analyses indicated a failure condition (SF = 1.0) when the water level approached the soil surface (Table 11).

3.5.1.5 Conceptual synthesis

The field failure situation presented a very elongated and highly three-dimensional geometry, a condition that is difficult to simulate in 2D analyses (more experimental data are needed for 3D analyses). Nevertheless, slope stability

Table 10. Shear strength equations and parameters from triaxial compression and direct shear tests.

Failure envelopes/ test type	c' (kPa)	ϕ' (º)	Obs.
1 – CID	3.6	36.9	undist.
2 – CID	7.2	31.6	undist. and remold.
3 – mix	13.9	31.6	undist.
4 – mix	-	36.9	remold.
DST	9.7	26.3	undist.
DST	4.5	25.8	remold.

Legend: CID = Consolidated isotropically drained; DST – Direct shear tests.

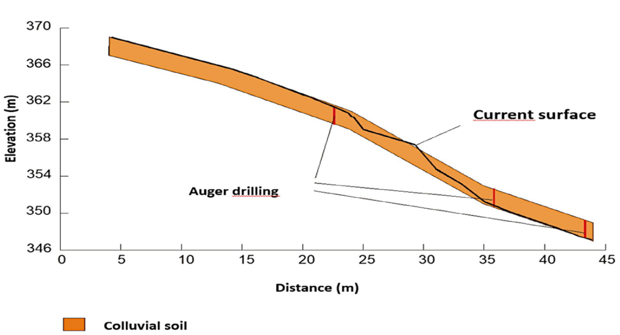

Figure 39. Geotechnical section used in flow analysis.

Table 11. Safety factors for infinite slopes in relation to the "water level".

i (º)	Z_w (cm) – (m)			
	0(0)	80 (0.4)	120 (0.6)	200 (1.0)
27	1.8	1.48	1.34	1.04
36	1.3	1.10	1.0	-

γ_t=15.8kN/m^3; m =(Z_w/Z).

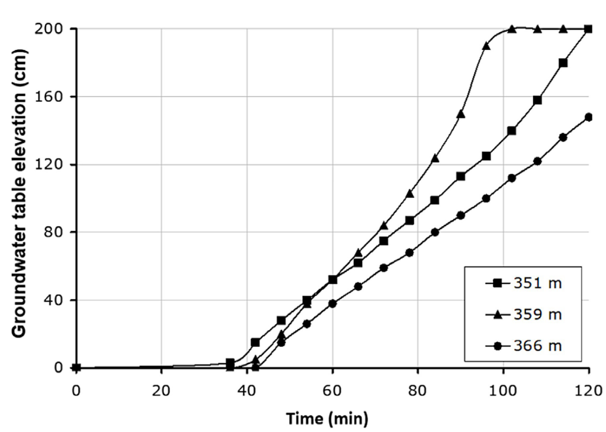

Figure 40. Results of flow analysis - elevation of the water table on 3 positions of the slope as a function of time.

CC BY

analyses, using the infinite slope method with parallel flow, indicated that the slope becomes unstable when Z_w reaches values between 1.2 m and 2.0 *m* (*m* = 0.6 - 1.0), depending on the slope considered. Flow analyses showed that the critical values of *m* (=*Zw/Z*) are reached after approximately 100 to 120 minutes for a rainfall like the one that occurred on the day of the failure, which corresponds well to eyewitness reports.

In summary, it can be stated that the experimental results allowed establishing an adequate flow simulation for the rainfall that occurred in December 2000. Respecting the limitations of the analysis methods, the measured resistance values explain the observed failure quite satisfactorily.

3.5.2 Gravitational mass movements that occurred in May 2024

Between May and June of 2024, Rio Grande do Sul experienced a catastrophic event with widespread flooding and mass movements affecting 478 of its 497 municipalities. Approximately 2.4 million people were impacted, over 600,000 displaced, 70,000 relocated to shelters, 800 injured, 183 killed, and 27 reported missing (Rio Grande do Sul, 2024).

Figure 41 maps rainfall accumulation from April 27 to May 19, showing 400–900 mm in the Guaíba Lake basin, with the highest concentration in the central region. Figure 42 highlights landslide scars (red) and flood zones (blue), revealing a strong correlation between heavy rainfall and mass movements.

The Joint Technical Note issued by IGEO/CEPSRM (October 2024) mapped 15,376 landslide scars and 16,862 rupture points over an area exceeding 18,000 km², based on high-resolution satellite imagery (Andrades-Filho & Mexias, 2024). The identified scars correspond to the combination of at least two distinct types of mass movement processes: rapid movements, which left well-defined scars and often evolved into debris flows; and slower movements, such as rotational landslides, characterized by smaller scars and lower displacement velocities. All processes were recorded across 150 municipalities, with notable concentrations in Caxias do Sul (656 scars), Veranópolis (636), and Agudo (540).

Analyses conducted by Egas et al. (2025) presented a mapping of landslide scars based on both satellite imagery and field surveys, aiming to identify the rupture, transport, and deposition zones. The authors concluded that most of the rupture points were primarily associated with translational landslides (with varying depths) and debris flows. These processes were identified over an area of approximately 63,000 km², equivalent to 22% of the territory of Rio Grande do Sul, resulting in significant social and material losses. Figure 43 illustrates a debris flow that occurred in 2024 along the thalweg in the Taquari-Antas Valley, leading to the destruction of a restaurant near the BR-470 bridge.

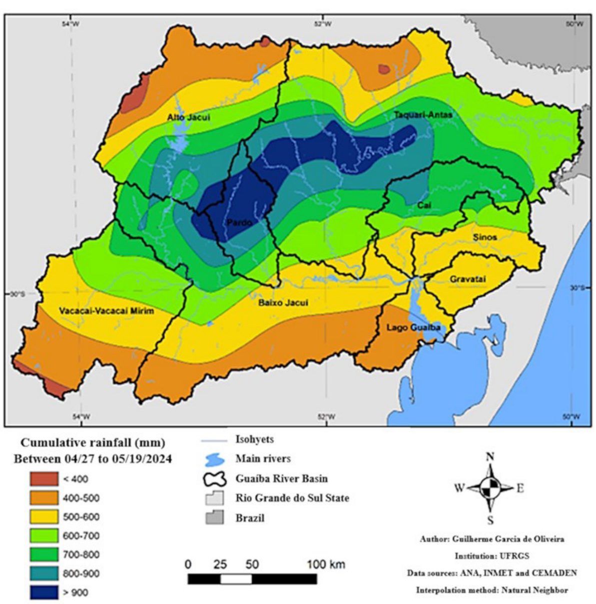

Figure 41. Distribution of accumulated rainfall between 04/27 and 05/19/2024 in the Guaíba lake basin (UFRGS, 2024).

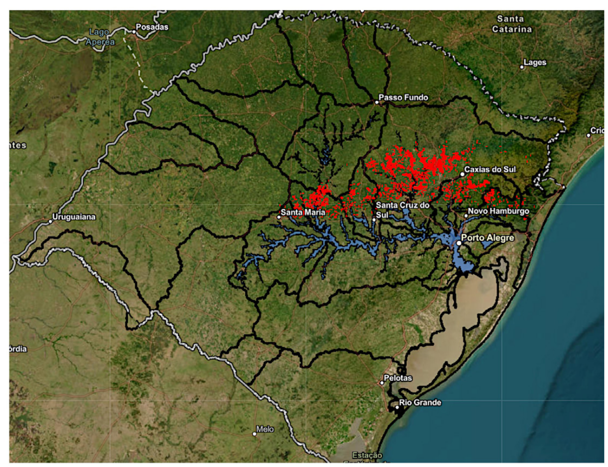

Figure 42. Distribution of GMM scars and flood areas (Andrades-Filho & Mexias, 2024).

Figure 43. Debris flow along the thalweg in the Taquari-Antas Valley, causing the destruction of a restaurant near the BR-470 bridge (2024).

The prolonged and intense rainfall triggered various mass movements. The Serra Gaúcha's inter-slide levels, with thick colluvium, experienced slow but damaging movements affecting roads and buildings. Steep slopes in the Antas and Caí river valleys saw hundreds of flat landslides that evolved into destructive debris flows. Figure 44 shows scenarios that occurred in many locations, with greater or lesser destruction.

Clarke et al. (2024) classified the 10-day and 4-day rainfall events as extremely rare, with return periods of 100–250 years. While El Niño contributed to rainfall variability, human-induced climate change has increased the probability of such extreme events.

The findings emphasize the need for stronger infrastructure, environmental policies, and risk management strategies. Improved forecasting and early warning systems, along with preventive actions, are crucial to minimizing the impact of future disasters.

4. Discussion and integration of results

This article analyzes 11 case studies across Brazilian states: four in Pernambuco, two in Rio de Janeiro, two in São Paulo, one in Paraná, and two in Rio Grande do Sul. These studies highlight the complexity of gravitational mass movements (GMM) and different approaches to understanding and mitigating their impacts. Each case study analyzes the predisposing, aggravating, and triggering factors, failure mechanisms, the analyses conducted, and the stabilization strategies implemented in infrastructure and urban settings. Table 12 presents a summary of the main information presented in each of the case studies.

The geology of the analyzed areas varies between residual granite and gneiss soils, Barreiras Formation sediments, and colluvial deposits. The main movements identified include translational and rotational slides, creep-type movements, debris flows, and block falls, with a focus on slides and creep. Field and laboratory investigations included SPT drillings, geophysical surveys, physical characterization, hydraulic conductivity, and shear strength tests to support numerical analyses and instability assessments.

Monitoring was conducted using piezometers, inclinometers, and rain gauges to understand soil behavior and identify critical conditions preceding mass movements.

Table 12. Summary of key geotechnical information from case studies.

Loc.[A]	Geol.	Movement[B]	Investigation[C]	Instr.[D]	Predisp. Factors	Trigg. Factors	Stability Analysis / Solutions
1	Residual soil Mica-rich gneiss	TL	SPT, HC, SC, DS	P	High mica, foliation	Excavation, rainwater	Back-analysis (Unsat.)
2	Residual soil of granite / Barreiras F. sediments	RL	SPT, HC, CMA, SC, DS	I, P, RG	Conductivity contrast	Anthropogenic action, rainwater, groundwater	Analysis / DHD, soil nailing, surface protection
3	Barreiras F. sediments	TL	SPT, HC, SC, DS	None	Steep slope, weak soil	Anthropogenic action, rainwater	3D Analysis
4	Barreiras F. sediments / Residual soil of granite	RL & TL	In development	RG	Under analysis	Anthropogenic action, rainwater	In development
5	Talus-colluvium	CM	SPT, GS, SC, DS	I, P, RG	Rugged slopes	Rainwater, groundwater	Deep Horiz. Piezometer
6	Talus-colluvium	CM	SPT, GS, SC, DS	I, P, RG	Permeable fractures	Rainwater, groundwater	Analysis / DHD
7	Not specified	NS	Not Specified	T	Exposed soil	Rainwater	Surface cover analysis
8	Colluvial deposit	CM	Not Specified	I, P	Low perm., Hydro complexity	Rainwater, groundwater, anthropogenic action	DHD, retaining structures
9	Clayey-silty colluvium	CM	Not Specified	I, P, RG	Low perm., Hydro complexity	Rainwater, groundwater	DHD
10	Heterogeneous colluvium	RTL	FHC, HC, DS, TST	P	Wavy relief	Rainwater, groundwater	Stability analysis
11	Not specified	L, DMF, RF, CM	In development	RG	Under analysis	Rainwater	In development

Legend: ALocation: 1 - Machados (PE-89); 2 - Camaragibe (PE); 3 - Alto do Padre Cícero (Camaragibe - PE); 4 - MR-Recife; 5 - BR-116 (km 101) - Serra do Mar (RJ); 6 - BR-116 (km 29) - Serra do Mar (RJ); 7 - São Paulo (SP); 8 - São Paulo - Vila Albertina (SP); 9 - Serra do Mar (PR); 10 - São Vendelino (RS); 11 - Rio Grande do Sul; BType of Movement: CM - Creep Movements; DMF - Debris & Mud Flows; L – Landslides; NS - Not Specified; RF – Rockfall; RL - Rotational Landslide; RTL - Rapid Translational Landslide; TL - Translational Landslide; CField and Laboratory Investigation: CMA - Chemical and Mineralogical Analyses; DS - Direct Shear; FHC - Field Hydraulic Conductivity Tests; GS - Geophysical Surveys; HC - Hydraulic Conductivity; SC - Soil Characterization; SPT – Standard Penetration Test; TST – Triaxial Shear Test; DInstrumentation: I – Inclinometer; P – Piezometer; RG - Rain Gauge; T – Tensiometer.

Figure 44. Landslide on slopes of Rio das Antas, near the BR470 bridge (Cleber Floriano).

Data revealed the influence of positive pore pressure on soil displacement, leading to mitigation efforts such as deep drainage systems (DHD).

Most case studies observed deep drainage as a primary stabilization strategy to counteract soil water infiltration. A study in São Paulo also demonstrated how surface protection helps maintain soil suction during rainy periods, stabilizing slopes and reducing seasonal effects on unsaturated soils.

The findings align with Cruden & Varnes (1996) and Augusto Filho et al. (2018), emphasizing geological and geomorphological factors as key predisposing elements in Brazilian GMM. For example, in Machado (PE), high mica content and foliation parallel to the slope create adverse soil discontinuities, while in São Valentino (RS), concave-convex slopes and intense river dissection contribute to instability.

Inadequate human interventions frequently act as aggravating factors. Unregulated cuts and fills, improper debris disposal, informal housing construction, and uncontrolled wastewater discharge contribute to slope weakening. In Camaragibe (PE), continuous wastewater discharge represents a persistent aggravating factor. In Machado (PE), excavations carried out without proper geotechnical investigation reduced the safety factor, increasing the slope's susceptibility to failure. Subsequently, intense rainfall triggered the landslide.

Rainwater infiltration remains the primary triggering factor, as soil moistening reduces suction, increasing failure risk. In many cases, raising the water table and generating positive pore pressure precedes displacement. Instrumentation in Pernambuco, Rio de Janeiro, São Paulo, and Paraná confirmed a strong correlation between precipitation and mass movements.

For example, at BR-116/km 29 in Rio de Janeiro, displacements increased when precipitation exceeded 250 mm over 25 days. In Vila Albertina (SP), accumulated rainfall of 320 mm in 30 days triggered movements. In Camaragibe (PE), a landslide reactivated when 100 mm of rain fell within 25 days. However, it is important to determine, in each case, the time necessary to cause slope failure.

5. Conclusion

Landslides are among the most frequent and deadly natural hazards in Brazil, causing severe environmental, economic, and social losses in infrastructure and urban areas. Case studies highlight rainwater infiltration and unregulated human activities as aggravating factors and primary triggers. Addressing these challenges requires:

- Geological-geotechnical investigations to identify the causes, understand failure mechanisms, and provide data for stability analyses and effective stabilization solutions.
- Monitoring systems to detect aggravating and triggering factors, assess seasonal impacts on unsaturated soils, and validate stabilization measures, ensuring timely maintenance.
- Numerical analyses to evaluate instability risks, particularly in unsaturated soils where safety factors fluctuate significantly during rainy seasons. Inadequate human interventions further exacerbate slope failures.
- Efficient drainage systems (both surface and deep), adequate surface protection, and cost-benefit analyses of retaining structures are essential. Planning should integrate urban development with preventive stabilization measures and infrastructure projects.
- Adaptation to climate change, as increasing extreme rainfall events demand new approaches that consider regional specificities in infrastructure, housing, and slope stabilization. Meteorological forecasting remains a key challenge.
- Legislation, technical standards, and public policies must be up-to-date and effective. Risk mapping, urban planning, infrastructure development, and coordinated risk management actions between government and communities are essential for integrated disaster management.

Brazil's growing exposure to extreme rainfall and human-induced vulnerabilities calls for proactive strategies that integrate engineering, monitoring, and policy efforts to mitigate landslide risks and promote safer urban development, as well as sustainable and resilient infrastructure.

Acknowledgements

The authors congratulate the Brazilian Association of Soil Mechanics for its 75 years of history and achievements. They also express their gratitude to the journal Soils and Rocks for the support received.

Declaration of interest

The authors have no conflicts of interest to declare. All co-authors have observed and affirmed the contents of the paper and there is no financial interest to report.

Authors' contributions

Roberto Quental Coutinho: conceptualization, data curation, formal analysis, funding acquisition, methodology, visualization, writing – original draft. Mauricio Ehrlich: conceptualization, formal analysis, funding acquisition, methodology, supervision, writing – review & editing. Marcos Massao Futai: conceptualization, formal analysis, funding acquisition, methodology, supervision, writing – review & editing. Luiz Antônio Bressani: conceptualization, formal analysis, funding acquisition, methodology, supervision, writing – review & editing. Willy Alvarenga Lacerda: conceptualization, formal analysis, funding acquisition, methodology, supervision, writing – review & editing. Bruno Diego de Morais: conceptualization, data curation, formal analysis, methodology, writing – original draft.

Data availability

The datasets generated and analyzed in the course of the current study are available from the corresponding authors upon request.

Declaration of use of generative artificial intelligence

This work was prepared with the assistance of generative artificial intelligence (GenAI) ChatGPT, with the objective of improving and condensing the text previously written by the authors. The entire process of using this tool was supervised, reviewed, and, when necessary, edited by the authors. The authors assume full responsibility for the content of the publication that involved the aid of GenAI.

List of symbols and abbreviations

c'	Effective cohesion
c^*	Apparent cohesion
i	Hydraulic gradient
m	Relationship Between Water Level and Soil Depth (=Zw/Z)
BFS	Barreiras Formation soil GRS granite residual soil
CEMADEN	National Center for Natural Disaster Monitoring and Alerts
DHD	Deep Horizontal Drains
DTM	Digital Terrain Model
GASBOL	Bolivia–Brazil Gas Pipeline
GMM	Gravitational Mass Movements
GRS	Granite residual soil
GS	Specific gravity
GWT	Groundwater table
K_{sat}	Hydraulic conductivity coefficient
LEM	Limit Equilibrium Method
LL	Liquid limit
LP	Plastic limit
N_{SPT}	Number of strokes in the SPT test
PI	Plasticity index
RQD	Rock Quality Designation
SF	Safety factor
SPT	Standard Penetration Tests
Z	Soil depth
β	Slope inclination
γ_s	Unit weight of the grains
γ_t	Unit weight of the soil
γ_w	Unit weight of the water
ϕ'	Effective friction angle
ϕ^b	Angle of the rate of increase in shear strength of unsaturated soil with respect to matric suction

References

Alves, G.J., Mello, C.R., Guo, L., & Thebaldi, M.S. (2022). Natural disaster in the mountainous region of Rio de Janeiro state, Brazil: assessment of the daily rainfall erosivity as an early warning index. *International Soil and Water Conservation Research*, 10, 547-556. http://doi.org/10.1016/j.iswcr.2022.02.002

Andrades-Filho, C.O., & Mexias, L.S.F. (2024). *WebMapa de Movimentos de Massa para equipes de apoio na situação de calamidade*. Universidade Federal do Rio Grande do Sul. Retrieved in January 10, 2025, from https://arcg.is/ezjvW

Augusto Filho, O. (1992). Caracterização geológico-geotécnica voltada a estabilização de encostas: uma proposta metodológica. In *Anais da I Conferência Brasileira Sobre Estabilidade de Encostas* (pp. 721-733). Rio de Janeiro. São Paulo: ABMS.

Augusto Filho, O., Virgili, J.C., & Diláscio, M.V. (2018). Estabilização de taludes. In A.M.S. Oliveira & J. Jerônimo (Eds.), *Geologia de engenharia e ambiental* (Vol. 2, pp. 400-420). ABGE.

Azambuja, E., Nanni, A.S., Bressani, L.A., Rigo, M.L., & Zeni, C.A. (2001). Avaliação dos fluxos de detritos em Alto Feliz no Rio Grande do Sul. In *Anais da III Conferência Brasileira sobre Estabilidade de Encostas*, Rio de Janeiro. São Paulo: ABMS.

Banco Mundial. (2012). *Avaliação de Perdas e Danos: Inundações e Deslizamentos na Região Serrana do Rio de Janeiro - Janeiro de 2011*. Banco Mundial.

Bandeira, A.P.N., & Coutinho, R.Q. (2015). Critical rainfall parameters: proposed landslide warning system for the Metropolitan Region of Recife, PE, Brazil. *Soils and Rocks*, 38(1), 27-48. http://doi.org/10.28927/SR.381027.

CC BY

Bauzys, F. (2010). *Identificação, análise e mapeamento dos movimentos de massa ocorridos em novembro de 2008, no alto da bacia do Ribeirão Nelchior Gaspar-SC* [Master's dissertation]. Federal University of Santa Catarina.

Bjerrum, L., & Huder, J. (1957). Measurement of the permeability of compacted clays. In *Proceedings of the 4th International Conference on Soil Mechanics and Foundation Engineering* (Vol. 1, pp. 6-8), London. ISSMGE.

Bressani, L.A., Martinello, I.A., Silveira, R.M., & Bica, A.V.D. (2006). Resultados de ensaios de condutividade hidráulica nos solos coluvionares de São Vendelino, RS. In *Anais do XIII Congr. Brasileiro de Mec. Solos e Eng. Geotécnica* (Vol. 2, pp. 769-774), Curitiba. São Paulo: ABMS.

Bromhead, E.N. (1992). *The stability of slopes*. Spon Press. http://doi.org/10.4324/9780203975350.

Clarke, B., Barnes, C., Rodrigues, R., Zachariah, M., Alves, L.M., Haarsma, R., Pinto, I., Yang, W., Vahlberg, M., Vecchi, G., Izquierdo, K., Kimutai, J., & Otto, F.E.L. (2024). *Climate change, El Niño and infrastructure failures behind massive floods in southern Brazil*. Imperial College London. http://doi.org/10.25561/111882.

Companhia de Pesquisa de Recursos Minerais – CPRM. (2000). *Geological map of the state of Rio de Janeiro* (R.F. 1:500,000). CPRM.

Costa, W.M. (2023). Storms and catastrophe in São Sebastião - SP at carnival 2023. *Confins*, 58, 1-11. http://doi.org/10.4000/confins.50176.

Coutinho, R.Q. (2024). *Ferramentas Geológicas-Geotécnicas Digitais e Monitoramento para Auxílio a Gestão Integrada de Risco em Encostas da Formação Barreiras em* Áreas *do Recife e Jaboatão dos Guararapes* (Relatório Técnico Final). Recife: Fundação de Amparo à Ciência e Tecnologia de Pernambuco.

Coutinho, R.Q., & Severo, R.N.F. (2009). Investigação geotécnica para projeto de estabilidade de encostas. In *Anais da V Conferência Brasileira de Estabilidade de Encostas* (pp. 1-55). São Paulo: ABMS.

Coutinho, R.Q., Morais, B.D., Oliveira, M.S., & Souza Neto, D.P. (2020). Alto do Padre Cícero Hillside 3D Stability Analysis in Camaragibe - PE/Brasil. In *Proceedings of the XIII International Symposium on Landslides* (pp. 1-9), Cartagena. ISSMGE.

Coutinho, R.Q., Neto, J.B.S., & Costa, F.Q. (2000). Design strength parameters of a slope on unsaturated gneissic residual soil. In *Proceedings of the Geo-Denver 2000* (pp. 247-261), Denver. ASCE. http://doi.org/10.1061/40510(287)17.

Coutinho, R.Q., Silva, M.M., Santos, A.N., & Lacerda, W.A. (2019). Geotechnical characterization and failure mechanism of landslide in granite residual soil. *Journal of Geotechnical and Geoenvironmental Engineering*, 145(8), 05019004. http://doi.org/10.1061/(ASCE)GT.1943-5606.0002052.

Coutinho, R.Q., Souza Neto, J.B., Santos, L.M., & Lafayette, K.P.V. (2006). Geotechnical characterization of an unsaturated soil in the Barreiras Formation, Pernambuco – Brazil. In *Proceedings of the Unsaturated soils 2006* (Vol. 1, pp. 1627-1638). ASCE.

Coutinho, R.Q.C., Morais, B.D., Mendes, R.M., & Andrade, M.R.M. (2023). Alert scenarios for the Metropolitan Region of Recife-PE based on monitoring of rainfall and soil humidity: a case study. *Soils and Rocks*, *46*(4), 1-12. Retrieved in January 15, 2025, from https://www.soilsandrocks.com/sr-2023-008323

Coutinho, R.Q.C., Silva, C.B.D., Gomes, E.C., Araújo Filho, J.C., & Silva, B.Q. (2024). A semi-detailed survey of soils in the city of Jaboatão dos Guararapes – PE: a contribution to the geotechnical mapping of suitability for urbanization. *Revista Brasileira de Geografia Física*, 17(6), 4328-4355. http://doi.org/10.26848/rbgf.v17.6.p4325-4352

Cruden, D.M., & Varnes, D.J. (1996). Landslide types and processes. In A.K. Turner & R.L. Schuster (Eds.), *Landslides: investigation and mitigation, transportation research board special report* (pp. 36-75). National Academy Press.

Du, J., Yin, K., & Lacasse, S. (2013). Displacement prediction in colluvial landslides, Three Gorges Reservoir, China. *Landslides*, *10*(2), 203-218. http://doi.org/10.1007/s10346-012-0326-8.

Egas, H.M., Stabile, R.A., Andrade, M.R.M., Michel, G.P., Araújo, J.P.C., Michel, R.D.L., Mendes, T.S.G., Nery, T.D., Paula, D.S., & Reckziegel, E.W. (2025). Comprehensive inventory and initial assessment of landslides triggered by autumn 2024 rainfall in Rio Grande do Sul, Brazil. *Landslides*, 22, 579-589. http://dx.doi.org/10.1007/s10346-024-02410-w.

Ehrlich, M., Costa, D.P., & Silva, R.C. (2018). Behavior of a colluvial slope located in Southeastern Brazil. *Landslides*, 15(8), 1595-1613. http://doi.org/10.1007/s10346-018-0964-6.

Ehrlich, M., Costa, D.P., & Silva, R.C. (2021). Long-term monitoring of the behavior of a talus-colluvium deposit. *Landslides*, 18(6), 2225-2245. http://doi.org/10.1007/s10346-021-01649-x.

Franch, F.A.J., & Futai, M.M. (2009). Influência da cobertura de superfície em fluxos não saturados. In *Anais da 5ª Conferência Brasileira sobre Estabilidade de Encostas*, São Paulo.

Franch, F.A.J., & Futai, M.M. (2010). Influência das variações sazonais da pressão da água na estabilidade de taludes não saturados. In *Proceedings of the Fifth Internacional Conference Unsaturated Soils*, Barcelona.

Fredlund, D.G., Xing, A., & Huang, S. (1994). Predicting the permeability function for unsaturated soils using the soil-water characteristic curve. *Canadian Geotechnical Journal*, 31(4), 533-546. http://doi.org/10.1139/t94-062.

Froude, M.J., & Petley, D.N. (2018). Global fatal landslide occurrence from 2004 to 2016. *Natural Hazards and Earth System Sciences*, 18(8), 2161-2181. http://doi.org/10.5194/nhess-18-2161-2018.

Gariano, S.L., & Guzzetti, F. (2016). Landslides in a changing climate. *Earth-Science Reviews*, 162, 227-252. http://doi.org/10.1016/j.earscirev.2016.08.011.

Godois, J.V.S., Ito, W.H., & Futai, M.M. (2009). Um caso de deslizamento ativo na Vila Albertina-SP. In *Anais da 5ª Conferência Brasileira sobre Estabilidade de Encostas*, São Paulo.

Goudie, A.S. (2004). *Encyclopedia of Geomorphology*. Routledge.

Highland, L.M., & Bobrowsky, P. (2008). The landslide handbook: A guide to understanding landslides. *Geological Survey Circular*, http://doi.org/10.3133/cir1325.

Hungr, O., Leroueil, S., & Picarelli, L. (2014). The Varnes classification of landslide types, an update. *Landslides*, 11(2), 167-194. http://doi.org/10.1007/s10346-013-0436-y.

Junho, M.C.B., & Penha, H.M. (1982). *Schematic geological section of the Serra dos Orgãos: sign located at km 89 of BR-116/RJ*. DRM-RJ - Departamento de Recursos Minerais do Rio de Janeiro.

Lacerda, W.A. (2004). The behavior of colluvial slopes in a tropical environment. In *Proceedings of the 9th International Symposium on Landslides* (pp. 315-1342), Rio de Janeiro. CRC Press. http://doi.org/10.1201/b16816-191.

Lacerda, W.A. (2007). Landslide initiation in saprolite and colluvium in southern Brazil: field and laboratory observations. *Geomorphology*, 87(3), 104-119. http://doi.org/10.1016/j.geomorph.2006.03.037.

Leroueil, S., Vaunat, J., Picarelli, L., Locat, J., Lee, H., & Faure, R. (1996). Geotechnical characterization of slope movements. In *Proceedings of the 7th International Symposium on Landslides* (pp. 27-48), Trondheim. ISSMGE.

Lu, N., & Godt, W. (2013). *Hillslope hydrology and stability*. Cambridge: Cambridge University Press. http://doi.org/10.1017/CBO9781139108164.

Macedo, E.S., & Sandre, L.H. (2022). Mortes por deslizamentos no Brasil: 1988 a 2022. *Revista Brasileira de Geologia de Engenharia e Ambiental*, 12(1), 110-117.

Marengo, J.A., Alcantara, E., Cunha, A.P., Seluchi, M., Nobre, C.A., Dolif, G., Gonçalves, D., Dias, M.A., Cuartas, L.A., Bender, F., Ramos, A.M., Mantovani, J.R., Alvalá, R.C., & Moraes, O.L. (2023). Flash floods and landslides in the city of Recife, Northeast Brazil after heavy rain on May 25-28, 2022: causes, impacts, and disaster preparedness. *Weather and Climate Extremes*, 39, 100545. http://doi.org/10.1016/j.wace.2022.100545.

Pereira, P.G.S., Coutinho, R.Q., Souza Neto, D.P., & Gomes, I.F. (2025). Stability analysis of an urban slope under human activities and critical rainfall: case study of Recife, Brazil. *Geotechnical and Geological Engineering*, 43(1), 68-86. http://doi.org/10.1007/s10706-024-03011-z.

Recife. Secretaria Executiva de Assistência Social – SUAS. (2023). *Boletim Informativo* nº 003/2023. Recife, PE: SUAS.

Rio Grande do Sul. Governo do Estado. (2024). *Defesa Civil atualiza balanço das enchentes no RS – 20/8*. Governo do Estado do Rio Grande do Sul. Retrieved in January 15, 2025, from https://www.estado.rs.gov.br/defesa-civil-atualiza-balanco-das-enchentes-no-rs-20-8

Rosi, A., Canavesi, V., Segoni, S., Nery, T.D., Catani, F., & Casagli, N. (2019). Landslides in the Mountain Region of Rio de Janeiro: a proposal for the semi-automated definition of multiple rainfall thresholds. *Geosciences*, 9(5), 1-15. http://doi.org/10.3390/geosciences9050203.

Silveira, R.M. (2008). *Comportamento Geotécnico de um Solo Coluvionar de São Vendelino (RS)* [Doctoral thesis]. Federal University of Rio Grande do Sul. Retrieved in January 15, 2025, from http://hdl.handle.net/10183/13519

Suzuki, S., Lacerda, W.A., & Futai, M.M. (2012). Estimativa de Parâmetros de Resistência para Estabilidade de uma Encosta com Base em Ensaios de Laboratório e Retro-Análise. In *Anais do Congresso Brasileiro de Mecânica dos Solos e Engenharia Geotécnica*, Porto de Galinas.

Suzuki, S., Lacerda, W., Freitas, N.C., Amaral, C.S., & Futai, M.M. (2013). Estudo de encostas monitoradas com oleoduto enterrado em massas coluvionares instáveis na Serra do Mar. In *Anais da VI Conferência Brasileira Sobre Estabilidade de Encostas* (pp. 538-545), Angra dos Reis. São Paulo: ABMS.

Universidade Federal do Rio Grande do Sul – UFRGS. Programa de Pós-graduação em Sensoriamento Remoto - PPGSR. (2024). *Pesquisador do PPGSR atua em mapeamentos e modelagem de* áreas *de inundação no RS*. Retrieved in January 15, 2025, from https://www.ufrgs.br/ppgsr/pesquisador-do-ppgsr-atua-em-mapeamentos-e-modelagem-de-areas-de-inundacao-no-rs/

Varnes, D.J. (1978). Slope movement types and processes. In R.L. Schuster & R.J. Krizek (Eds.), *Landslides: analysis and control* (Special Report, Vol. 176, pp. 11-33). Washington, D.C.: National Academy of Sciences.

Vasconcelos Junior, F.C., Zachariah, M., Silva, T.L.V., Santos, E.P., Coelho, C.A.S., Alves, L.M., Passos, E.S., Martins, R., Koberle, A.C., Singh, R., Vahlberg, M., Marchezini, V., Heinrich, D., Thalheimer, L., Raju, E., Koren, G., Philip, S.Y., Kew, S.F., Bonnet, R., Li, S., Yang, W., Sun, J., Vecchi, G., & Otto, F.E.L. (2024). An attribution study of very intense rainfall events in Eastern Northeast Brazil. *Weather and Climate Extremes*, 45, 1-16. http://doi.org/10.1016/j.wace.2024.100699.

World Meteorological Organization - WMO. (2021). *WMO atlas of mortality and economic losses from weather, climate and water extremes (1970-2019)*. WMO.

CC BY